JOURNAL OF MATHEMATICAL SCIENCES AND MODELLING

ISSN: 2636-8692

VOLUME V
ISSUE II

VOLUME V ISSUE II
ISSN 2636-8692

August 2022
http://dergipark.gov.tr/jmsm

JOURNAL OF MATHEMATICAL SCIENCES AND MODELLING

Editors

Editorial Board of Journal of Mathematical Sciences and Modelling

Contents

Journal of Mathematical Sciences and Modelling, 5 (2) (2022) 40-47
Research Article

Journal of Mathematical Sciences and Modelling

Journal Homepage: www.dergipark.gov.tr/jmsm
ISSN 2636-8692
DOI: http://dx.doi.org/10.33187/jmsm.1080204

Stability and Boundedness of Solutions of Nonlinear Third Order Differential Equations with Bounded Delay

Erdal Korkmaz[1*] **and Abdulhamit Özdemir**[1]

[1]*Mathematics, Faculty of Arts and Sciences, Muş Alparslan University, 49100, Muş, Turkey*
[*]*Corresponding author*

Article Info

Keywords: *Boundedness, Delay differential equations, Lyapunov functional, Stability, Third order*
2010 AMS: *34C11, 93D20*
Received: *28 February 2022*
Accepted: *4 April 2022*
Available online: *30 August 2022*

Abstract

In this paper, we investigate the boundedness and uniformly asymptotically stability of the solutions to a certain third order non-autonomous differential equations with bounded delay. By constructing a Lyapunov functional, sufficient conditions for the stability and boundedness of solutions for equations considered are obtained. We used an example to demonstrate the feasibility of our results. The results essentially improve, include, and complement the results in the literature.

1. Introduction

For years, researchers have focused on the qualitative behavior of differential equation solutions, such as stability, asymptotic stability, uniform asymptotic stability, boundedness, and uniform boundedness. In the application areas of mathematics such as physics, chemistry, biology, engineering and dynamical systems, many events are modeled with differential equations [1, 2]. The qualitative behavior of the differential equations corresponding to these models is important and finds concrete responses in the application areas [3]-[5]. Also, the rapid expansion of differential equations with lag arguments in recent years and now covers not only many physics and technology questions, but also certain areas of economics and biological sciences [6, 7]. Therefore, the qualitative behavior of the solutions of differential equations with delay arguments remains up-to-date and attracts the attention of many researchers.
The fact that the trajectory curve of a solution starting in a region does not leave this region is known as the stability of the solution [8]. A great advantage of the method known as Lyapunov's second method for determining the stability behavior of solutions of linear and nonlinear systems is to examine the stability of the solutions without any prior knowledge of the solutions [9]. The simplest form of third-order differential equations is of the form

$$x''' + ax'' + bx' + cx = 0 \tag{1.1}$$

where a, b, c are constants. In this case it is well known that all solutions tend to the trivial solution, as $t \to \infty$ provided that the Routh-Hurwitz criteria $a > 0, c > 0, ab - c > 0$ are satisfied [10]. In [10], author obtains sufficient conditions for the asymptotic stability of the trivial solution of differential equations of the form

$$x''' + f(x,x')x'' + g(x') + h(x) = 0 \tag{1.2}$$

considering the criteria Routh-Hurwitz for equation (1.1).
In [11]-[19], the authors investigated the behavior of solutions of differential equations such as asymptotic stability, global asymptotic stability, global stability, boundedness, uniform boundedness in different third-order nonlinear models using the Lyapunov method.
In [20], the author constructed some new Lyapunov functions to examine the asymptotic stability and boundedness of the solutions of non-linear delay differential equation described by

$$x''' + a(t)x'' + b(t)x' + c(t)f(x(t-r)) = p(t) \tag{1.3}$$

***Email addresses and ORCID numbers*: e.korkmaz@alparslan.edu.tr, 0000-0002-6647-9312 (E. Korkmaz), abdulhamitozdemir@hotmail.com, 0000-0002-5310-6285 (A. Özdemir)**

with $p \equiv 0$ and $p \neq 0$, respectively. In [21], the authors established sufficient conditions for the asymptotic stability and boundedness of solutions of a certain third order nonlinear non-autonomous delay differential equation described by

$$[g(x(t))x'(t)]'' + a(t)x''(t) + b(t)x'(t)) + c(t)f(x(t-r)) = p(t) \tag{1.4}$$

with $p(t) \equiv 0$ and $p(t) \neq 0$, respectively. In recent years [22]-[33], the authors obtained remarkable results by using the Lyapunov method of the behavior of the solutions of differential equations with or without delay in different third-order nonlinear models. For detailed information on the behavior of solutions of third order lagged or undelayed differential equations, references and their references can be consulted.
Inspired by the studies above, especially by expanding the scope of [21], that is, the behavior of the solutions of a new equation is examined by taking the delay variable and the coefficients as the functions of the dependent variable.
In this paper, we investigate the uniform asymtotic stability of the solutions for $p(t,x,x',x'') \equiv 0$ and additionally boundedness of solutions to the third order nonlinear differential equation with bounded delay

$$[P(x(t))x'(t)]'' + a(t)(Q(x(t))x'(t))' + b(t)(R(x(t))x'(t)) + c(t)f(x(t-r(t))) = p(t,x,x',x''). \tag{1.5}$$

For convenience, we let

$$\theta_1(t) = \frac{P'(x(t))}{P^2(x(t))}x'(t),$$

$$\theta_2(t) = \frac{Q'(x(t))P(x(t)) - Q(x(t))P'(x(t))}{P^2(x(t))}x'(t),$$

and

$$\theta_3(t) = \frac{R'(x(t))P(x(t)) - R(x(t))P'(x(t))}{P^2(x(t))}x'(t).$$

We write (1.5) in the system form

$$\begin{aligned} x' &= \frac{1}{P(x)}y, \\ y' &= z, \\ z' &= -a(t)\theta_2(t)y - \frac{a(t)Q(x)}{P(x)}z - \frac{b(t)R(x(t))y}{P(x(t))} - c(t)f(x(t)) + c(t)\int_{t-r(t)}^{t} \frac{1}{P(x)}f'(x)yd\eta + p(t,x,y,z) \end{aligned} \tag{1.6}$$

where r is a bounded delay, $0 \leq r(t) \leq \Omega$, $r'(t) \leq \lambda$, $0 < \lambda < 1$, λ and Ω some positive constants, Ω which will be determined late, the functions a,b,c are continuously differentiable functions and the functions P,Q,R,f,p are continuous functions depending only on the arguments shown. Also derivatives $P'(x),P''(x),Q'(x),R'(x)$ and $f'(x)$ exist and are continuous, $f(0) = 0$. The continuity of the functions a,b,c,P,Q,R,f and p guarantees the existence of the solutions of equation (1.5). If the right hand side of the system (1.6) satisfies a Lipchitz condition in $x(t),y(t),z(t)$ and $x(t-r(t))$ and exists of solutions of system (1.6) , then it is unique solution of system (1.6).
Assume that there are positive constants $a_0,b_0,c_0,p_0,q_0,r_0,a_1,b_1,c_1,,p_1,q_1,$ and r_1 such that the following assumptions hold:

(A1) $0 < a_0 \leq a(t) \leq a_1$, $0 < b_0 \leq b(t) \leq b_1$ and $0 < c_0 \leq c(t) \leq c_1$ for all $t \geq 0$;
(A2) $0 < p_0 \leq P(x) \leq p_1$, $0 < q_0 \leq Q(x) \leq q_1$, and $0 < r_0 \leq R(x) \leq r_1$ for $x \in \mathbb{R}$;
(A3) $\frac{f(x)}{x} \geq \delta_0 > 0$ for $x \neq 0$ and $|f'(x)| \leq \delta_1$ for all x; and
(A4) $|p(t,x,y,z)| \leq |e(t)|$.

Using the Lyapunov's functional approach, we establish some new results on the uniformly asymtotically stability and boundedness of the solutions, which are motivated by the results of references. Our results differ from those existing in the literature (see, references and the references therein). By this way, we mean that this work offers to the literature on the subject and may be significant for researchers who study the qualitative behaviour of solutions of higher-order functional differential equations. The uniqueness and originality of the present paper can be checked based on all of the above facts.

2. Preliminaries

We also consider the functional differential equation

$$\dot{x} = f(t,x_t), \;\; x_t(\theta) = x(t+\theta), \;\; -r \leq \theta \leq 0, \;\; t \geq 0 \tag{2.1}$$

where $f : I \times C_H \to \mathbb{R}^n$ is a continuous mapping, $I = [0,\infty)$, $f(t,0) = 0$, $C_H := \{\phi \in (C[-r,0],\mathbb{R}^n) : \|\phi\| \leq H\}$, and for $H_1 < H$, there exists $L(H_1) > 0$, with $|f(t,\phi)| < L(H_1)$ when $\|\phi\| < H_1$.

Lemma 2.1. *([5]) Let $V(t,\phi) : I \times C_H \to \mathbb{R}$ be a continuous functional satisfying a local Lipchitz condition, $V(t,0) = 0$, and wedges W_i such that :*

(i) $W_1(\|\phi\|) \leq V(t,\phi) \leq W_2(\|\phi\|)$;
(ii) $V'_{(3)}(t,\phi) \leq -W_3(\|\phi\|)$.

Then, the zero solution of equation (2.1) is uniformly asymptotically stable.

3. The Main Results

Theorem 3.1. *In addition to the basic assumptions imposed on the functions a,b,c,P,Q,R and e suppose that there are positive constants δ_0,δ_1,η_1 and η_2 such that the following conditions are satisfied:*

(i) $\frac{p_1\delta_1}{r_0} < d < a_0q_0$;
(ii) $c(t) \le b(t)$ *and* $b'(t) \le c'(t) \le 0$ *for* $t \in [0,\infty)$;
(iii) $\frac{1}{2}da'(t)Q(x) - b_0(dr_0 - p_1\delta_1) \le -\varepsilon < 0$;
(iv) $\int_{-\infty}^{\infty}(|P'(u)| + |Q'(u)| + |R'(u)|)du \le \eta_1 < \infty$; *and*
(v) $\int_0^{\infty}|e(s)|\,ds \le \eta_2 < \infty$.

Then any solution $x(t)$ equation (1.5) are bounded and trival solution of equation (1.5) for $p(t,x,x',x'') \equiv 0$ is uniformly asymtotically stability, if

$$\Omega < \frac{2p_0}{p_1c_1\delta_1}\min\left\{\frac{\varepsilon(1-\lambda)p_0}{p_1\left(p_0+d(2-\lambda)\right)},\ (a_0q_0-d)\right\}. \tag{3.1}$$

Proof. To prove the theorem, we define a Lyapunov functional

$$W = W(t,x,y,z) = exp\left(\frac{-1}{\eta}\int_0^t \gamma(s)ds\right)V, \tag{3.2}$$

where

$$\gamma(t) = |\theta_1(t)| + |\theta_2(t)| + |\theta_3(t)|, \tag{3.3}$$

and

$$V = V(t,x,y,z) = dc(t)F(x) + c(t)f(x)y + \frac{b(t)R(x)}{2P(x)}y^2 + \frac{1}{2}z^2 + \frac{1}{2}\frac{da(t)Q(x)}{P^2(x)}y^2 + \frac{d}{P(x)}yz + \sigma\int_{-r(t)}^0\int_{t+s}^t y^2(\gamma)d\gamma ds \tag{3.4}$$

with $F(x) = \int_0^x f(s)ds$, and η are positive constants that will be determined at a later point of the proof. We can write V as

$$V = dc(t)F(x) + M(x,y) - \frac{c^2(t)P(x)f^2(x)}{2b(t)R(x)} + \frac{1}{2}z^2 + \frac{d}{P(x)}yz + \frac{da(t)Q(x)}{2P^2(x)}y^2 + \sigma\int_{-r(t)}^0\int_{t+s}^t y^2(\gamma)d\gamma ds$$

where

$$M(x,y) = \frac{b(t)R(x)}{2P(x)}\left\{y + \frac{c(t)f(x)P(x)}{b(t)R(x)}\right\}^2 \ge 0.$$

Note that

$$\frac{1}{2}f^2(x) = \int_0^x f(u)f'(u)du \le \int_0^x f(u)\delta_1 du$$

and

$$\sigma\int_{-r(t)}^0\int_{t+s}^t y^2(\gamma)d\gamma ds \ge 0.$$

From conditions (A1)–(A3) and (ii), we have

$$-\frac{c^2(t)P(x)f^2(x)}{2b(t)R(x)} \ge -\frac{c(t)}{b(t)}\frac{c(t)p_1}{r_0}\frac{f^2(x)}{2} \ge -\frac{c(t)p_1}{r_0}\delta_1\int_0^x f(u)du.$$

Hence,

$$V \quad \ge \quad dc(t)\int_0^x\left(1-\frac{p_1\delta_1}{dr_0}\right)f(u)du + \frac{1}{2}\left(z+\frac{d}{P(x)}y\right)^2 + \frac{d(a_0q_0-d)}{2P^2(x)}y^2 \ge \frac{\delta_4\delta_0}{2}x^2 + \frac{1}{2}\left(z+\frac{d}{P(x)}y\right)^2 + \frac{d(a_0q_0-d)}{2P^2(x)}y^2,$$

where $\delta_4 = dc_0\left(1-\frac{p_1\delta_1}{dr_0}\right) > 0$ by (i). So we can find a constant $d_0 > 0$ small enough, such that

$$V \ge d_0(x^2+y^2+z^2). \tag{3.5}$$

It is clear that $V(t,x,y,z) \geq 0$ and $V(t,0,0,0) = 0$ if and only if $x^2 = y^2 = z^2 = 0$. Now contidions (A2) and (iv) imply

$$\begin{aligned}\int_0^t \gamma(s)ds &\leq (1+r_1+q_1)\int_{\alpha_1(t)}^{\alpha_2(t)} \frac{|P'(u)|}{P^2(u)}du + \int_{\alpha_1(t)}^{\alpha_2(t)} \frac{|R'(u)|+|Q'(u)|}{P^2(u)}du \\ &\leq \frac{(1+r_1+q_1)}{p_0^2}\int_{\alpha_1(t)}^{\alpha_2(t)} |P'(u)|du + \frac{1}{p_0}\int_{\alpha_1(t)}^{\alpha_2(t)} (|R'(u)|+|Q'(u)|)du \\ &\leq N < \infty, \end{aligned} \tag{3.6}$$

where $\alpha_1(t) = \min\{x(0), x(t)\}$ and $\alpha_2(t) = \max\{x(0), x(t)\}$. Hence,

$$W \geq D_0(x^2+y^2+z^2) \tag{3.7}$$

for some $D_0 > 0$. Also, from (A1)–(A3), it is not difficult to see that

$$W \leq D_1(x^2+y^2+z^2), \tag{3.8}$$

for all x, y, and z.
From (3.7), and (3.8), it is easy to see that $W(t,x,y,z) = 0$ if and only if $x^2+y^2+z^2 = 0$ for all $t \geq 0$, and $W(t,x,y,z) > 0$ if $x^2+y^2+z^2 \neq 0$. Now, we illustrate that $\dot{W}$ is a negative definite function. The derivative of the function V along any solution $(x(t), y(t), z(t))$ of system (1.6), with respect to t is after rearranging

$$\begin{aligned}\frac{d}{dt}V(t) &= \left[\frac{da'(t)Q(x) + 2c(t)P(x)f'(x) - 2db(t)R(x)}{2P^2(x)}\right]y^2 \\ &\quad + V_1(t) + V_2(t) + \frac{1}{P(x)}(d - a(t)Q(x))z^2 + \sigma r(t)y^2(t) - \sigma(1-r'(t))\int_{t-r(t)}^{t} y^2(\eta)d\eta \\ &\quad + c(t)\left(\frac{d}{P(x)}y + z\right)\int_{t-r(t)}^{t} \frac{1}{P(x)}f'(x)yd\eta + \left(\frac{d}{P(x)}y + z\right)p(t,x,y,z)\end{aligned}$$

where

$$\begin{aligned}V_1 &= dc'(t)F(x) + c'(t)yf(x) + \frac{b'(t)R(x)}{2P(x)}y^2 \\ V_2 &= -d\theta_1(t)\left(yz + \frac{a(t)Q(x)}{2P(x)}y^2\right) + \frac{b(t)}{2}\theta_3(t)y^2 - a(t)\theta_2(t)\left(yz + \frac{d}{2P(x)}y^2\right).\end{aligned}$$

By regarding conditions (A2), (A3), and (ii), we have the following

$$da'(t)Q(x) + 2c(t)P(x)f'(x) - 2db(t)R(x) \leq da'(t)Q(x) + 2c(t)P(x)\delta_1 - 2db(t)r_0 \leq da'(t)Q(x) + 2b(t)(p_1\delta_1 - dr_0).$$

From (A1), (A2), (i) and (iii), and using the inequality $2ab \leq a^2+b^2$, we can rearrange

$$\begin{aligned}V'(t) &\leq V_1(t) + V_2(t) - \left(\frac{\varepsilon}{p_1^2} - \sigma r(t) - \frac{d\delta_1 c_1 r(t)}{2p_0^2}\right)y^2 - \left(\frac{1}{p_1}(a_0q_0 - d) - \frac{\delta_1 c_1 r(t)}{2p_0}\right)z^2 \\ &\quad + \left(\frac{\delta_1 c_1 p_0 + d\delta_1 c_1}{2p_0^2} - \sigma(1-\lambda)\right)\int_{t-r(t)}^{t} y^2(\eta)d\eta + \left(\frac{d}{P(x)}|y| + |z|\right)|p(t,x,y,z)|\end{aligned} \tag{3.9}$$

By choosing $\sigma = \frac{\delta_1 c_1 p_0 + d\delta_1 c_1}{2p_0^2(1-\lambda)}$, we have

$$\begin{aligned}V'(t) &\leq -\left(\frac{\varepsilon}{p_1^2} - \frac{\delta_1 c_1 p_0 + d\delta_1 c_1(2-\lambda)}{2p_0^2(1-\lambda)}\Omega\right)y^2 - \left(\frac{1}{p_1}(a_0q_0 - d) - \frac{\delta_1 c_1}{2p_0}\Omega\right)z^2 \\ &\quad + V_1(t) + V_2(t) + \left(\frac{d}{P(x)}|y| + |z|\right)|p(t,x,y,z)|.\end{aligned} \tag{3.10}$$

We claim that $V_1(t) \leq 0$. To show this we distinguish two cases. If $c'(t) = 0$, then $V_1 = \frac{b'(t)R(x)}{2P(x)}y^2 \leq 0$.
If $c'(t) < 0$, then we can write

$$\begin{aligned}V_1(t) &= dc'(t)\left[F(x) + \frac{1}{d}yf(x) + \frac{b'(t)R(x)}{2dP(x)c'(t)}y^2\right] \\ &= dc'(t)\left[F(x) + \frac{b'(t)R(x)}{2dP(x)c'(t)}\left\{y + \frac{c'(t)P(x)f(x)}{b'(t)R(x)}\right\}^2 - \frac{c'(t)P(x)f^2(x)}{2db'(t)R(x)}\right],\end{aligned}$$

from which condition (ii) implies

$$\begin{aligned} V_1(t) &\leq dc'(t)\int_0^x \left(1-\frac{P(x)f'(u)}{dR(x)}\right) f(u)du \\ &\leq dc'(t)\int_0^x \left(1-\frac{p_1\delta_1}{dr_0}\right) f(u)du \\ &\leq c'(t)\frac{\delta_4}{c_0}F(x) \leq 0. \end{aligned}$$

Combining the two cases, we have $V_1(t) \leq 0$.
Using the inequality $2ab \leq a^2+b^2$, we obtain the estimate

$$\begin{aligned} V_2 &\leq \left[\frac{d}{2}|\theta_1(t)|\left(1+\frac{a_1q_1}{p_0}\right)+\frac{a_1}{2}|\theta_2(t)|\left(1+\frac{d}{p_0}\right)\right](y^2+z^2)+\frac{b_1}{2}|\theta_3(t)|y^2 \\ &\leq k_1(|\theta_1(t)|+|\theta_2(t)|+|\theta_3(t)|)(y^2+z^2), \end{aligned}$$

where $k_1 = \max\left\{\frac{d}{2}\left(1+\frac{a_1q_1}{p_0}\right), \frac{a_1}{2}\left(1+\frac{d}{p_0}\right), \frac{b_1}{2}\right\}$. Using these estimates for V_1 and V_2 in (3.10), we obtain

$$V'(t) \leq -D_2\left(y^2+z^2\right)+k_1(|\theta_1(t)|+|\theta_2(t)|+|\theta_3(t)|)(y^2+z^2)+\left(\frac{d}{P(x)}y+z\right)p(t,x,y,z) \tag{3.11}$$

where $D_2 = \min\left\{\frac{\varepsilon}{p_1^2}-\frac{\delta_1c_1p_0+d\delta_1c_1(2-\lambda)}{2p_0^2(1-\lambda)}\Omega,\ \frac{1}{p_1}(a_0q_0-d)-\frac{\delta_1c_1}{2p_0}\Omega\right\}$.
From (A4), (3.5), (3.6), (3.7), (3.11) and the Cauchy Schwartz inequality, we get

$$\begin{aligned} \dot{W}_{(2)} &= \left(\dot{V}_{(2)}-\frac{1}{\eta}\gamma(t)V\right)exp\left(\frac{-1}{\eta}\int_0^t\gamma(s)ds\right) \\ &\leq \left(-D_2\left(y^2+z^2\right)+\left(\frac{d}{P(x)}y+z\right)p(t,x,y,z)\right)exp\left(\frac{-1}{\eta}\int_0^t\gamma(s)ds\right) \\ &\leq \left(\frac{d}{p_0}|y|+|z|\right)|p(t,x,y,z)| \\ &\leq D_3\left(2+y^2+z^2\right)|e(t)| \\ &\leq D_3\left(2+\frac{1}{D_0}W\right)|e(t)| \\ &\leq 2D_3|e(t)|+\frac{D_3}{D_0}W|e(t)|, \end{aligned} \tag{3.12}$$

where $D_3 = \max\left\{\frac{d}{p_0},1\right\}$, $\eta = \frac{d_0}{k_1}$. Using the Gronwall inequality and the condition (v) and integrating inequalty (3.12) from 0 to t, we have

$$\begin{aligned} W &\leq W(0,x(0),y(0),z(0))+2D_3\eta_2+\frac{D_3}{D_0}\int_0^t W(s,x(s),y(s),z(s))|e(s)|ds \\ &\leq (W(0,x(0),y(0),z(0))+2D_3\eta_2)exp\left(\frac{D_3}{D_0}\int_0^t|e(s)|ds\right) \\ &\leq (W(0,x(0),y(0),z(0))+2D_3\eta_2)exp\left(\frac{D_3}{D_0}\eta_2\right) = K_1 < \infty \end{aligned} \tag{3.13}$$

Because of inequalities (3.7) and (3.13), we write

$$\left(x^2+y^2+z^2\right) \leq \frac{1}{D_0}W \leq K_2, \tag{3.14}$$

where $K_2 = \frac{K_1}{D_0}$. Clearly (3.14) imlies that

$$|x(t)| \leq \sqrt{K_2},\ |y(t)| \leq \sqrt{K_2},\ |z(t)| \leq \sqrt{K_2} \text{ for all } t \geq 0.$$

That is

$$|x(t)| \leq \sqrt{K_2},\ \ |x'(t)| \leq \sqrt{K_2},\ \ |x''(t)| \leq \sqrt{K_2} \text{ for all } t \geq 0 \tag{3.15}$$

which completes the proof boundedness solutions of equation (1.5).
Now we show that the solutions of equation (1.5) for $p(t,x,x',x'') \equiv 0$ is uniformly asymtotically stability. The inequality (3.12) can write as

$$\begin{aligned} \dot{W}_{(2)} &= \left(\dot{V}_{(2)}-\frac{1}{\eta}\gamma(t)V\right)e^{-\frac{1}{\eta}\int_0^t\gamma(s)ds} \\ &\leq -D_2\left(y^2+z^2\right)e^{-\frac{1}{\eta}\int_0^t\gamma(s)ds} \\ &\leq -\mu(y^2+z^2), \end{aligned}$$

where $\mu = D_2e^{-\frac{N}{\eta}}$. It can also be observed that the unique solution of system (1.6) for which $\dot{W_{(2)}}(t,x,y,z,w) = 0$ is the solution $x = y = z = 0$.
Due to the the above discussion, the trival solution of the equation system (1.6) is uniformly asymptotically stable. □

Example 3.2. *We consider the following third order non-autonomous nonlinear differential equation with delay*

$$\begin{aligned}&\left[\left(\frac{x\cos x}{7(1+x^6)}+2\right)x'\right]''+\left(\frac{e^{-t}\cos t}{4}+\frac{1}{2}\right)\left(\left(\frac{x^2\sin x}{7(1+x^6)}+3\right)x'\right)'+\left(\frac{1}{2+t^6}+1\right)\left(\frac{x}{2(e^{2x}+e^{-2x})}+\frac{21}{10}\right)x'\\&+\frac{1}{50}\left(\frac{1}{3+t^6}+\frac{1}{4}\right)\left(x(t-\frac{1}{e^t+100})+\frac{x(t-\frac{1}{e^t+100})}{1+x^6(t-\frac{1}{e^t+100})}\right)\\&=\frac{2\sin t}{t^2+1+x^2+(x'x'')^2}\end{aligned}\tag{3.16}$$

where $P(x)=\frac{x\cos x}{7(1+x^6)}+2$, $Q(x)=\frac{x^2\sin x}{7(1+x^6)}+3$, $R(x)=\frac{x}{2(e^{2x}+e^{-2x})}+\frac{21}{10}$, $f(x)=x+\frac{x}{1+x^6}$, $r(t)=\frac{1}{e^t+100}$, $a(t)=\frac{e^{-t}\cos t}{4}+\frac{1}{2}$, $b(t)=\frac{1}{2+t^6}+1$, $c(t)=\frac{1}{3+t^6}+\frac{1}{4}$, $p(t)=\frac{2\sin t}{t^2+1+x^2+(x'x'')^2}$.

It is easy to see that $p_0=1$, $p_1=3$, $q_0=1$, $q_1=3$, $r_0=2$, $r_1=\frac{7}{3}$, $a_0=0.25$, $a_1=0.75$, $b_0=1$, $b_1=1.5$, $c_0=0.25$, $c_1=\frac{7}{12}$

$$\delta_0=\frac{1}{50}\le\frac{f(x)}{x}=\frac{1}{50}\left(1+\frac{1}{1+x^2}\right)\quad for\quad x\neq 0,\quad |f'(x)|\le\frac{1}{25}=\delta_1,$$

$$\frac{p_1\delta_1}{r_0}=\frac{3}{50}<d<\frac{1}{4}=a_0q_0,$$

and

$$\frac{1}{2}da'(t)Q(x)-b_0(dr_0-p_1\delta_1)\le-\frac{d}{8}+\frac{3}{25}<0\quad for\quad d=\frac{1}{10}.$$

Also we have

$$\int_0^{+\infty}|a'(t)|dt=\int_0^{+\infty}\left|\frac{-e^{-t}\cos t-e^{-t}\sin t}{4}\right|dt\le\int_0^{+\infty}\frac{2}{4}e^{-t}dt=\frac{1}{2},$$

$$\begin{aligned}\int_{-\infty}^{+\infty}|P'(u)|du&=\frac{1}{7}\int_{-\infty}^{+\infty}\left|\frac{(\cos u-u\sin u)(1+u^6)-6u^6\cos u}{(1+u^6)^2}\right|du\\&=\frac{1}{7}\int_{-\infty}^{+\infty}\left|\frac{\cos u}{1+u^6}-\frac{u\sin u}{1+u^6}-\frac{6u^6\cos u}{(1+u^6)^2}\right|du\\&\le\frac{1}{7}\int_{-\infty}^{+\infty}\left[\frac{7}{1+u^6}+\frac{u^2}{1+u^6}\right]du\\&=\frac{5}{7}\pi,\end{aligned}$$

$$\begin{aligned}\int_{-\infty}^{+\infty}|Q'(u)|du&=\frac{1}{7}\int_{-\infty}^{+\infty}\left|\frac{(2u\sin u+u^2\cos u)(1+u^6)-6u^7\sin u}{(1+u^6)^2}\right|du\\&=\frac{1}{7}\int_{-\infty}^{+\infty}\left|\frac{2u\sin u}{1+u^6}+\frac{u^2\cos u}{1+u^6}-\frac{6u^7\sin u}{(1+u^6)^2}\right|du\\&\le\frac{1}{7}\int_{-\infty}^{+\infty}\left[\frac{3u^2}{1+u^6}+\frac{6u^8}{(1+u^6)^2}\right]du\\&=\frac{2}{7}\pi,\end{aligned}$$

$$\begin{aligned}\int_{-\infty}^{+\infty}|R'(u)|du&=\frac{1}{2}\int_{-\infty}^{+\infty}\left|\frac{(e^{2u}+e^{-2u})-2u(e^{2u}-e^{-2u})}{(e^{2u}+e^{-2u})^2}\right|du\\&=\frac{1}{2}\int_0^{+\infty}\left[\frac{1}{e^{2u}+e^{-2u}}+2u\frac{e^{2u}-e^{-2u}}{(e^{2u}+e^{-2u})^2}\right]du+\frac{1}{2}\int_{-\infty}^{0}\left[\frac{1}{e^{2u}+e^{-2u}}+2u\frac{e^{2u}-e^{-2u}}{(e^{2u}+e^{-2u})^2}\right]du\\&=\frac{\pi}{4},\end{aligned}$$

and

$$\begin{aligned}\int_0^{+\infty}|p(t,x,x',x'')|dt&\le\int_0^{+\infty}|\frac{2\sin t}{t^2+1+x^2+(x'x'')^2}|dt\\&\le\int_0^{+\infty}\left|\frac{2\sin t}{t^2+1}\right|dt\\&\le\int_0^{+\infty}\frac{2}{t^2+1}dt\\&=\pi\end{aligned}$$

As a result, all of Theorem assumptions hold, indicating that any solution $x(t)$ *equation (3.16) are bounded and trival solution of equation (3.16) for* $p(t,x,x',x'')\equiv 0$ *is uniformly asymtotically stability.*

4. Conclusion

For the asymptotic stability of solutions of a class of nonlinear differential equation systems with bounded delay is obtained new sufficient conditions using a theorem presented in this paper. Since the special cases of our equation are the studies done in the literature, our results include the present results. The effectiveness of the theorem is demonstrated using an example.

Acknowledgements

The authors would like to express their sincere thanks to the editor and the anonymous reviewers for their helpful comments and suggestions.

Funding

There is no funding for this work.

Availability of data and materials

Not applicable.

Competing interests

The authors declare that they have no competing interests.

Author's contributions

All authors contributed equally to the writing of this paper. All authors read and approved the final manuscript.

References

[1] V. B. Kolmanovskii, V. R. Nosov, *Stability of functional-differential equations, Mathematics in Science and Engineering,* **180**, Academic Press, Inc. [Harcourt Brace Jovanovich, Publishers], London, 1986.
[2] V. Kolmanovskii, A. Myshkis, *Introduction to the Theory and Applications of Functional Differential Equations*, Kluwer Academic Publishers, Dordrecht, 1999.
[3] T. A. Burton, *Stability and Periodic Solutions of Ordinary and Functional Differential Equations*, Mathematics in Science and Engineering, Vol. 178, Academic Press, Orlando, 1985.
[4] J. Hale, *Theory of Functional Differential Equations*, Springer-Verlag, New York-Heidelberg, 1977.
[5] R. Reissig, G. Sansone, R. Conti, *Non-Linear Differential Equations of Higher Order*, Noordhoff International Publishing, Leyden, 1974.
[6] L. È. Èl'sgol'ts, *Introduction to the Theory of Differential Equations with Deviating Arguments*, Translated from the Russian by Robert J. McLaughlin Holden-Day, Inc., San Francisco, Calif.-London-Amsterdam, 1966.
[7] L. È. Èl'sgol'ts, S. B. Norkin, *Introduction to the Theory and Application of Differential Equations with Deviating Arguments*, Translated from the Russian by John L. Casti. Mathematics in Science and Engineering, Vol. 105. Academic Press [A Subsidiary of Harcourt Brace Jovanovich, Publishers], New York, London, 1973.
[8] N. N. Krasovskii, *Stability of Motion, Applications of Lyapunov's Second Method to Differential Systems and Equations with Delay*, Translated by J. L. Brenner Stanford University Press, Stanford, Calif. 1963.
[9] A. M. Lyapunov, *The General Problem of the Stability of Motion*, Translated from Edouard Davaux's French translation (1907) of the 1892 Russian original and edited by A. T. Fuller. Taylor & Francis, Ltd., London, 1992.
[10] J. O. C. Ezeilo, *On the stability of solutions of certain differential equations of the third order*, Quart. J. Math. Oxford Ser., **11**(2) (1960), 64-69.
[11] K. Swick, *On the boundedness and the stability of solutions of some nonautonomous differential equations of the third order*, J. London Math. Soc., **44** (1969), 347-359.
[12] K. E. Swick, *Asymptotic behavior of the solutions of certain third order differential equations*, SIAM J. Appl. Math. **19** (1970), 96-102.
[13] T. Hara, *On the asymptotic behavior of solutions of certain of certain third order ordinary differential equations*, Proc. Japan Acad., **47** (1971), 903-908.
[14] H. O. Tejumola, *A note on the boundedness and the stability of solutions of certain third-order differential equations*, Ann. Mat. Pura Appl., **92**(4) (1972), 65-75.
[15] T. Hara, *On the asymptotic behavior of the solutions of some third and fourth order non-autonomous differential equations*, Publ. Res. Inst. Math. Sci., **9**(74) (1973), 649-673.
[16] T. Hara, *On the asymptotic behavior of solutions of certain non-autonomous differential equations*, Osaka J. Math., **12** (1975), 267-282.
[17] T. Hara, *On the uniform ultimate boundedness of the solutions of certain third order differential equations*, J. Math. Anal. Appl., **80** (1981), 533-544.
[18] Y. F. Zhu, *On stability, boundedness and existence of periodic solution of a kind of third order nonlinear delay differential system*, Ann. Differential Equations, **8**(2) (1992), 249-259.
[19] C. Qian, *On global stability of third-order nonlinear differential equations*, Nonlinear Anal. **42** (2000), 651-661.
[20] M. O. Omeike, *Stability and boundedness of solutions of some non-autonomous delay differential equation of the third order*, An. Stiint. Univ. Al. I. Cuza Iasi. Mat. (NS), **55**(1) (2009), 49-58.
[21] M. Remili, L. D. Oudjedi, *Stability and boundedness of the solutions of nonautonomous third order differential equations with delay*, Acta Univ. Palack. Olomuc. Fac. Rerum Natur. Math., **53** (2014), 139-147.
[22] C. Tunç, *On the asymptotic behavior of solutions of certain third-order nonlinear differential equations*, J. Appl. Math. Stoch. Anal., **1** (2005), 29-35.
[23] C. Tunç, *Uniform ultimate boundedness of the solutions of third-order nonlinear differential equations*, Kuwait J. Sci. Engrg., **32** (2005), 39-48.
[24] C. Tunç, *Boundedness of solutions of a third-order nonlinear differential equation*, J. Inequal. Pure Appl. Math., **6**(1) (2005), Article 3, 1-6.
[25] B. S. Ogundare, G. E. Okecha, *On the boundedness and the stability of solution to third order non-linear differential equations*, Ann. Differential Equations, **24** (2008), 1-8.
[26] C. Tunç, *The boundedness of solutions to nonlinear third order differential equations*, Nonlinear Dyn. Syst. Theory, **10** (2010), 97-102.
[27] A. T. Ademola, P. O. Arawomo, *Asymptotic behaviour of solutions of third order nonlinear differential equations*, Acta Univ. Sapientiae Math., **3** (2011), 197-211.
[28] L. Zhang, L. Yu, *Global asymptotic stability of certain third-order nonlinear differential equations*, Math. Methods Appl. Sci., **36** (2013), 1845-1850.
[29] M. Remili, D. Beldjerd, *On the asymptotic behavior of the solutions of third order delay differential equations*, Rend. Circ. Mat. Palermo, **63**(2) (2014), 447-455.
[30] L. Oudjedi, D. Beldjerd, M. Remili, *On the stability of solutions for nonautonomous delay differential equations of third-order*, Differential Equations and Control Processes, **2014** (2014), 22-34.
[31] E. I. Verriest, A. Woihida, *Stability of nonlinear differential delay systems*, Math. Comput. Simul., **45**(3-4), (1998), 257-267.

[32] J. R. Graef, D. L. Oudjedi, M. Remili, *Stability and square integrability of solutions of nonlinear third order differential equations*, Dyn. Continuous Discrete Impulsive Syst. Ser. A: Math. Anal., **22** (2015), 313-324.
[33] J. R. Graef, D. Beldjerd, M. Remili, *On stability, ultimate boundedness, and existence of periodic solutions of certain third order differential equations with delay*, Panam. Math. J., **25** (2015), 82-94.

Journal of Mathematical Sciences and Modelling, 5 (2) (2022) 48-56
Research Article

Journal of Mathematical Sciences and Modelling

Journal Homepage: www.dergipark.gov.tr/jmsm
ISSN 2636-8692
DOI: http://dx.doi.org/10.33187/jmsm.1073324

Application of Mathematical Modeling in Multi Criteria Decision Making Process: Intuitionistic Fuzzy PROMETHEE

Feride Tuğrul[1*] **and Mehmet Çitil**[1]

[1]*Department of Mathematics, Kahramanmaraş Sütçü İmam University, Kahramanmaraş, Turkey*
[*]*Corresponding author*

Article Info

Keywords: *Intuitionistic fuzzy PROMETHEE, Intuitionistic fuzzy theory, Multi criteria decision making, Selection and evaluation in education*
2010 AMS: *03E72,90B50*
Received: *14 February 2022*
Accepted: *10 May 2022*
Available online: *30 August 2022*

Abstract

In this paper, the intuitionistic fuzzy PROMETHEE method is explained in detail and an original application has been made. The aim of the paper is to bring innovation to the evaluation system in the field of education by using the intuitionistic fuzzy PROMETHEE method. The advantages of using the PROMETHEE method, which is one of the many methods used in multi-criteria decision-making problems, in the intuitionistic fuzzy sense are explained in detail. Intuitionistic fuzzy PROMETHEE is a method that attracts our attention thanks to its benefits such as allowing the researcher to observe the positive and negative rankings simultaneously, expressing the degree of hesitation, changing the significance weights of the criteria, and using different methods when identifying the significance levels for each criterion, putting the degree of hesitation of significance weights into action, and enabling decision-makers, who are given the opportunity to use different criteria types and different criteria types for alternatives and criteria, to establish a unique system; moreover, the method also provides us numerous advantages while using it in our application area. It is of great importance for decision-makers to determine the specific importance level for each criterion. In this paper, controlled sets are used to express the importance of the criteria in the form of intuitionistic fuzzy values. The intuitionistic fuzzy-based PROMETHEE algorithm, aiming to contribute to the education system by examining the factors affecting the students' achievement, is a unique algorithm, and it is the first to shed light on various researchers.

1. Introduction

The main purpose of this paper is to explain the intuitionistic fuzzy PROMETHEE method and present an application that demonstrates the usefulness of the method. In addition, there is an example to improve the evaluation system, which is a first in the field of education, in this application where the intuitionistic fuzzy PROMETHEE method is used. This paper, it is aimed to create an intuitionistic fuzzy logic-based intelligent assessment system in which factors affecting students' success at the same time with their exam results are also activated. In order to create a training module suitable for individuals, a multi-criteria decision-making (MCDM) algorithm in intuitionistic fuzzy logic has been created using the PROMETHEE (Preference Ranking Organization Method for Enrichment of Evaluations) method. Creating a new algorithm with PROMETHEE method, it is aimed to solve this MCDM problem in the healthiest way with the help of the intuitionistic fuzzy theory-based PROMETHEE method. With the algorithm we did present, it is aimed to evaluate students' success not only according to the exam results, but also by considering their psychological, economic, social, and talented characteristics. Fuzzy logic was firstly defined by Zadeh in 1965 [1]. Then, the Intuitionistic fuzzy set (shortly IFS) was defined by K. Atanassov [2, 3]. If we give a brief information about these issues; we cannot say that every situation is completely true-false, good-bad as a fact and the problem. Therefore, the classical (Aristotle) logic used is insufficient in solving our problems or in situations we encounter. "There are shades of gray between black and white." According to the fuzzy logic that can be explained with the sentence, we can solve more of the problems we encounter in daily life. Fuzzy logic is built on the foundations of classical logic to include classical logic. While the studies on fuzzy logic were continuing, researchers encountered events in which they realized that fuzzy logic was also insufficient and that hesitation should have value in the

Email addresses and ORCID numbers: **feridetugrul@gmail.com, 0000-0001-7690-8080 (F. Tuğrul), citil@ksu.edu.tr, 0000-0003-3899-3434 (M. Çitil)**

decision-making process. The IF logic concept, which has proven useful for the solution of these and similar problems, is defined. Smart systems become more meaningful and applicable since the IFS includes the degree of membership, non-membership and hesitation. Since IFS also includes uncertainty, they are used in decision-making for incompletely defined and incomplete data, allowing us to obtain more consistent results. Intuitionistic fuzzy logic is based on fuzzy logic. As can be seen here, classical, fuzzy and intuitionistic fuzzy logic are intertwined. Intuitionistic fuzzy logic is a generalization of fuzzy logic. Intuitionistic fuzzy logic comes into play in situations where fuzzy logic cannot respond or is insufficient.The intuitionistic fuzzy set theory is useful in various application areas such as; medicine, medical diagnosis, medical application, career determination, real-life situations, education, decision making, multi-criteria decision making, artificial intelligence, networking, computer, smart systems, economy, and various fields. The decision-making process involves choosing between two or more choices. Multi-criteria decision-making (MCDM) is a well-known notion that aims to choose the best solution among various alternatives in decision-making. The working style of all MCDM methods is as follows: the Selection of Criteria, the Selection of Alternatives, the Selection of Aggregation Methods, and ultimately the Determination of Ranking which is based on weights or outranking [4]. Some of the MCDM methods are Analytical Hierarchy Process (AHP), Fuzzy Multi-Criteria Decision Making Process, ELECTRE, PROMETHEE, and the TOPSIS Method. Bellman and Zadeh were the first researchers who introduced decision-making in fuzzy logic. Multi-criteria fuzzy decision-making has been one of the rapidly growing areas in recent years thanks to its practicality. In MCDM problems, usually, the best alternative is chosen from those depending on the criteria. One of the multi-criteria decision-making methods PROMETHEE was developed by Jean Pierre Brans (1982) [5]. Using the PROMETHEE method could be taken a partial or complete ranking of alternatives based on the positive outranking flow, the negative outranking flow, and the net outranking flow. This method is different from other decision methods because it evaluates each alternative within itself. The main idea of PROMETHEE is to derive a partial or complete ranking of alternatives based on the positive outranking flow, the negative outranking flow, and the net outranking flow. Then it has been expanded in different forms. After being defined in the fuzzy field, it has been expanded in the sense of the intuitionistic fuzzy field. Many researchers have developed applications using PROMETHEE methods and intuitionistic fuzzy sets [6]- [16].

2. Preliminaries

Definition 2.1. *[2, 3] Let $X \neq \emptyset$. An intuitionistic fuzzy set A in X;*

$$A = \{\langle x, \mu_A(x), \nu_A(x)\rangle |\ x \in X\},$$

$$\mu_A(x), \nu_A(x), \pi_A(x) : X \to [0,1]$$

defined membership, nonmembership and hesitation degree of the element $x \in X$ respectively.

$$\mu_A(x) + \nu_A(x) + \pi_A(x) = 1.$$

Intuitionistic fuzzy value (IFV) defined by Xu [17]. Intuitionistic fuzzy value (IFV) is shown as follows: $\tilde{a} = (\mu_{\tilde{a}}, \nu_{\tilde{a}}, \pi_{\tilde{a}})$, where $\mu_{\tilde{a}}, \nu_{\tilde{a}}, \pi_{\tilde{a}} \in [0,1]$.
For each IFS $\tilde{A}$;

$$\pi_{\tilde{A}} = 1 - \mu_{\tilde{A}} - \nu_{\tilde{A}}. \tag{2.1}$$

In this paper; we will not write the third part so we'll show $\tilde{a} = (\mu_{\tilde{a}}, \nu_{\tilde{a}})$ shape instead of $\tilde{a} = (\mu_{\tilde{a}}, \nu_{\tilde{a}}, \pi_{\tilde{a}})$. The degree of hesitation can be obtained by equation (2.1).
For IFVs $\tilde{a} = (\mu_{\tilde{a}}, \nu_{\tilde{a}})$ and $\tilde{b} = (\mu_{\tilde{b}}, \nu_{\tilde{b}})$ the following operations have been carried out [17, 18]:

$$(1) \quad \tilde{a} \oplus \tilde{b} = \left(\mu_{\tilde{a}} + \mu_{\tilde{b}} - \mu_{\tilde{a}}\mu_{\tilde{b}}, \nu_{\tilde{a}}\nu_{\tilde{b}}\right) \tag{2.2}$$

$$(2) \quad \tilde{a} \otimes \tilde{b} = \left(\mu_{\tilde{a}}\mu_{\tilde{b}}, \nu_{\tilde{a}} + \nu_{\tilde{b}} - \nu_{\tilde{a}}\nu_{\tilde{b}}\right) \tag{2.3}$$

$$(3) \quad \oplus_{j=1}^{m} \tilde{a}_j = \left(1 - \prod_{j=1}^{m}(1-\mu_j), \prod_{j=1}^{m} \nu_j\right) \tag{2.4}$$

$$(4) \quad \otimes_{j=1}^{m} \tilde{a}_j = \left(\prod_{j=1}^{m} \mu_j, \prod_{j=1}^{m}(1-\nu_j)\right) \tag{2.5}$$

Many researchers have suggested approaches for comparing the IFVs [18, 19]. The following method will be used in this paper. This method was proposed by Szmidt and Kacprzyk, which leads to more consistent results than other methods [19]. This function is used to rank IFVs:

$$\rho(\alpha) = 0.5(1 + \pi_\alpha)(1 - \mu_\alpha)) \tag{2.6}$$

As the $\rho(\alpha)$ value decreases, the preferred value α increases.

2.1. The intuitionistic fuzzy PROMETHEE

When a MCDM problem is encountered, the decision maker is expected to choose the best alternative among the alternatives according to certain criteria. However, the significance of all the criteria can vary. In such cases, the weighting of the criteria shall be taken into consideration. The benefit of the PROMETHEE method is to assess considering the weight of the criterion. The criteria's weights indicate how important they are. Considering both intuitionistic fuzzy sets and weights of criteria at the same time, more consistent and rational results will be obtained. Therefore; using intuitionistic fuzzy PROMETHEE method will provide advantageous results. The criteria's weights could be depicted as IFVs: $\tilde{w}_j$ where $\mu_{\tilde{w}_j} \in [0,1], \nu_{\tilde{w}_j} \in [0,1], \mu_{\tilde{w}_j} + \nu_{\tilde{w}_j} \leq 1, j = 1,2,...,m$. According to the weights, $\mu_{\tilde{\omega}_j}$ and $\nu_{\tilde{\omega}_j}$ demonstrate the membership and non-membership degrees of the alternative x_i respectively. Indeed; the concept of weight represents

the importance of that criteria. The weights are expressed as IFV in the intuitionistic fuzzy PROMETHEE. It is of great importance for decision-makers to determine the specific importance level for each criterion. In this paper, controlled sets are used to express the importance of the criteria in the intuitionistic fuzzy PROMETHEE method in the form of intuitionistic fuzzy values. Some methods can help decision makers in determining intuitionistic fuzzy weights [20–25]. The basic definitions for controlled sets are as follows:

Definition 2.2. *[22] Let E be an universe, α is a function from E to I then E is called $\alpha-$ set.*

Definition 2.3. *[22] Let E be an $\alpha-$ set. The set E is called $\alpha-$ controlled set if*

$$\forall x \in E, \exists y \in E \ni 1-\alpha(x) = \alpha(y).$$

The family of $\alpha-$ controlled set on an universe E is represented by $E \in CS(\alpha)$.

Definition 2.4. *[22] Let $E \in CS(\alpha)$ and $a \in E$. The following set is called control set of a,*

$$\bar{a} = \{b \in E | 1-\mu(a) = \mu(b)\}$$

Definition 2.5. *[21] Let E be an $\alpha-$ set. We define the following mapping on E so that*

$$\alpha^*(x) = \begin{cases} 1-\alpha(x), & x \in E_\alpha \\ sup_y \alpha(y), & y \in E \ni \alpha(x) < 1-\alpha(y) \\ 0, & otherwise. \end{cases} \tag{2.7}$$

where $E_\alpha = \cup_{a \in E} \bar{a}$.

Definition 2.6. *[21] Let E be $\alpha-$ set. Then the set $A = \{\langle x, \alpha(x), \alpha^*(x)\rangle | x \in E\}$ is called $(\alpha, \alpha^*)-$ controlled set.*

In this research, V shape criterion type has been used [26]:

$$P(d) = \begin{cases} 0, & d \le q \\ \frac{d-q}{p-q}, & q < d \le p \\ 1, & d > p \end{cases} \tag{2.8}$$

Parameter thresholds q and p are indicated as indifference and strict preference, respectively. Decision makers are free to change these thresholds according to the desired situation. Evaluate the alternatives $x_i (i = 1,2,...,n)$ with respect to the criteria $c_j (j = 1,2,...,m)$ and determine the deviations based on pairwise comparisons:

$$d_j(x,y) = c_j(x) - c_j(y) \tag{2.9}$$

where $d_j(x,y)$ shows the distinction between the alternatives' the assessments x and y on the criterion c_j.

The decision maker first determines the assessment values of each alternative relative to different criteria and creates the paired preferences via the preference function, , which is also called as the general criterion in the classical PROMETHEE. There are six different types of generalized criteria. The preferences are limited in $[0,1]$ by the generalized criterion. If these preference functions are handled with a fuzzy set, membership functions and preference values are represented by $P_j(x,y)$. Besides preference values can be taken directly as fuzzy numbers as they are limited to $[0,1]$. However, with the help of the fuzzy set, only the preferred density defined by the membership function can be expressed. It is more convenient for the decision maker to use intuitionistic fuzzy set because it addresses all aspects of the criteria. Also with the help of intuitionistic fuzzy set, PROMETHEE method is more advantageous. Since; the intuitionistic fuzzy set could express not only the intensity of preferred but also the degrees of non-preferred and uncertain.

Definition 2.7. *[27] An intuitionistic fuzzy preference relation R on the set $X = x_1, x_2, ..., x_n$ is represented by a matrix $R = (r_{ik})_{n \times n}$, where $r_{ik} = \langle (x_i, x_k), \mu(x_i, x_k), \nu(x_i, x_k)\rangle$ for all $i,k = 1,2,...,n$. For convenience, we let $r_{ik} = (\mu_{ik}, \nu_{ik})$ where μ_{ik} denotes the degree to which the object x_i is preferred to the object x_k, ν_{ik} indicates the degree to which the object x_i is not preferred to the object x_k, and $\pi(x_i, x_k) = 1-\mu(x_i, x_k)-\nu(x_i, x_k)$ is interpreted as an indeterminacy degree or a hesitancy degree, with the condition:*

$$\mu_{ik},\ \nu_{ik} \in [0,1],\ \mu_{ik}+\nu_{ik} \le 1,\ \mu_{ik} = \nu_{ki},\ \mu_{ki} = \nu_{ik},\ \mu_{ii} = \nu_{ii} = 0.5,\ \pi_{ik} = 1-\mu_{ik}-\nu_{ik},\ for\ all\ i,k = 1,2,...,n. \tag{2.10}$$

2.2. Algorithm of intuitionistic fuzzy PROMETHEE

The preferences μ_{ik} between the alternatives x_i and x_k according to the criterion c_j could be calculated by Equations (2.9) and (2.8), and then the preference matrix according to the criterion c_j is obtained as follows [28]:

$$U^{(j)} = (\mu_{ik}^{(j)})_{n \times n} = \begin{bmatrix} - & \mu_{12}^{(j)} & \dots & \mu_{1n}^{(j)} \\ \mu_{21}^{(j)} & - & \dots & \mu_{2n}^{(j)} \\ \vdots & \vdots & - & \vdots \\ \mu_{n1}^{(j)} & \mu_{n2}^{(j)} & \dots & - \end{bmatrix} \tag{2.11}$$

Using the equations $\nu_{ki} = \mu_{ik}$ and $\nu_{ik} = \mu_{ki}$, the nonmembership degree of an IFV could be obtained. Matrix of the intuitionistic fuzzy preference relation is as follows:

$$R^{(j)} = (r_{ik}^{(j)})_{n \times n} = \begin{bmatrix} - & (\mu_{12}^{(j)}, \nu_{12}^{(j)}) & \dots & (\mu_{1n}^{(j)}, \nu_{1n}^{(j)}) \\ (\mu_{21}^{(j)}, \nu_{21}^{(j)}) & - & \dots & (\mu_{2n}^{(j)}, \nu_{2n}^{(j)}) \\ \vdots & \vdots & - & \vdots \\ (\mu_{n1}^{(j)}, \nu_{n1}^{(j)}) & (\mu_{n2}^{(j)}, \nu_{n2}^{(j)}) & \dots & - \end{bmatrix} \tag{2.12}$$

Then; considering the $c_j(j=1,2,\ldots,m)$ criteria, we must establish the general preference index for each alternative. We can get what we want by using weighted aggregation operators. There are a number of aggregation operators for intuitionistic fuzzy sets, such as the IFWA, IFWG, IFOWA, IFOWG, IFHA and IFHG operators [17, 18]. We will use the IFWA operator in this paper. The all intuitionistic fuzzy preference index of the alternative x_i to x_k on all criteria can be derived as:

$$r(x_i,x_k)=r_{ik}=\bigoplus_{j=1}^{m}\left(\tilde{w}_j\bigotimes r_{ik}^{(j)}\right) \tag{2.13}$$

where $r(x_i,x_k)=r_{ik}$ shows the degree to which the alternative x_i is preferred to the alternative x_k all criteria. Also, r_{ik} is an IFV. $\tilde{w}_j=(\mu_{\tilde{w}j},\nu_{\tilde{w}j})$, then according to Equation (2.2), (2.3):

$$\tilde{w}_j\bigotimes r_{ik}^{(j)}=\left(\mu_{ik}^{(j)}\mu_{\tilde{w}j},\nu_{ik}^{(j)}+\nu_{\tilde{w}j}-\nu_{ik}^{(j)}\nu_{\tilde{w}j}\right) \tag{2.14}$$

If Equations (2.4), (2.13) and (2.14) are combined;

$$\begin{aligned} r(x_i,x_k) &= \bigoplus_{j=1}^{m}\left(\tilde{w}_j\bigotimes r_{ik}^{(j)}\right) \\ &= \left(1-\prod_{j=1}^{m}(1-\mu_{ik}^{(j)}\mu_{\tilde{w}j}),\prod_{j=1}^{m}(\nu_{ik}^{(j)}+\nu_{\tilde{w}j}-\nu_{ik}^{(j)}\nu_{\tilde{w}j})\right) \end{aligned}$$

Overall intuitionistic fuzzy preference relationship is established as follows:

$$R=(r_{ik})_{n\times n}=\begin{bmatrix} - & (\mu_{12},\nu_{12}) & \ldots & (\mu_{1n},\nu_{1n}) \\ (\mu_{21},\nu_{21}) & - & \ldots & (\mu_{2n},\nu_{2n}) \\ \vdots & \vdots & - & \vdots \\ (\mu_{n1},\nu_{n1}) & (\mu_{n2},\nu_{n2}) & \ldots & - \end{bmatrix} \tag{2.15}$$

Every alternative is compared to option $(n-1)$. As a result of intuitionistic fuzzy positive and negative outranking flow can be achieved as follows:

(1) The intuitionistic fuzzy positive outranking flow:

$$\tilde{\varphi}^{+}(x_i)=\frac{1}{n-1}\bigoplus_{k=1,k\neq i}^{n}r(x_i,x_k)=\frac{1}{n-1}\bigoplus_{k=1,k\neq i}^{n}r_{ik} \tag{2.16}$$

(2) The intuitionistic fuzzy negative outranking flow:

$$\tilde{\varphi}^{-}(x_i)=\frac{1}{n-1}\bigoplus_{k=1,k\neq i}^{n}r(x_k,x_i)=\frac{1}{n-1}\bigoplus_{k=1,k\neq i}^{n}r_{ki} \tag{2.17}$$

The relationship between $\tilde{\varphi}^{+}(x_i)$ and $\tilde{\varphi}^{-}(x_i)$ can be explained with the help of Equation (2.6). The intuitionistic fuzzy net cannot be obtained by directly subtraction the outranking flow. The difference between the intuitionistic fuzzy positive and negative outranking flow can be calculated using the function defined by Szmidt and Kacprzyk.

$$\rho(\varphi(x_i))=\rho(\tilde{\varphi}^{+}(x_i))-\rho(\tilde{\varphi}^{-}(x_i)) \tag{2.18}$$

Three different ranking for $\tilde{\varphi}^{+}(x_i)$ and $\tilde{\varphi}^{-}(x_i)$ can be achieved [28]:

(1) Partial ranking: x_i outranks x_k if $\tilde{\varphi}^{+}(x_i)\geq\tilde{\varphi}^{+}(x_k)$ and $\tilde{\varphi}^{-}(x_i)\leq\tilde{\varphi}^{-}(x_k)$;
(2) Equality: $\tilde{\varphi}^{+}(x_i)=\tilde{\varphi}^{+}(x_k)$ and $\tilde{\varphi}^{-}(x_i)=\tilde{\varphi}^{-}(x_k)$ hold at the same time involves indifference between two options.
(3) Incomparability: This takes if $\tilde{\varphi}^{+}(x_i)>\tilde{\varphi}^{+}(x_k)$ and $\tilde{\varphi}^{-}(x_i)>\tilde{\varphi}^{-}(x_k)$ or $\tilde{\varphi}^{+}(x_i)<\tilde{\varphi}^{+}(x_k)$ and $\tilde{\varphi}^{-}(x_i)<\tilde{\varphi}^{+}(x_k)$.

If incomparability happens, intuitionistic fuzzy net outranking flow can be obtained by the help of Equation (2.18).

2.3. General algorithm

In this section, the steps of the algorithm that can be applied in every field are explained in detail. The algorithm we need to use when we want the best, the most accurate and the smartest solution, where the importance of the criteria are different, multiple criteria and alternatives are together, is given below by explaining all the steps. This algorithm is an algorithm that has an application area in all areas of multi-criteria decision making and will give us the most accurate result in any situation. At the same time, by using this algorithm in our study, we have shown its application and usefulness in the field of education. When we want to choose among alternatives with more than one criteria, not only in the field of education, this algorithm is used to make the best choice and the most accurate ranking among the alternatives. The general algorithm for the intuitionistic fuzzy PROMETHEE have been created as follows [16]:

Step 1: Alternatives $X=x_1,x_2,\ldots,x_n$ to be evaluated are determined. And criteria $C=c_1,c_2,\ldots,c_m$ that are important to evaluate alternatives are determined.

Step 2: The importance degree of the criteria is determined $\tilde{w}_j(j=1,2,\ldots,m)$ where $\mu_{\tilde{w}_j}+\nu_{\tilde{w}_j}\leq 1,\mu_{\tilde{w}_j}\in[0,1],\ \ \nu_{\tilde{w}_j}\in[0,1]$.

Step 3: The parameters q as an indifference threshold and p as a strict preference threshold are determined. Deviations $d_j(x,y)$ using

Equation (2.9), the preferences $\mu_{ik}^{(j)}$ for the alternative x_i against alternative x_k with respect to the criterion c_j by using the V-shape with indifference criterion are calculated. Then, the preference matrix $U^{(j)}(j=1,2,\ldots,m)$ are created.
Step 4: The intuitionistic fuzzy preference relation $R^{(j)}=(r_{ik}^{(j)})_{n\times n}$ is created.
Step 5: The overall intuitionistic fuzzy preference relation $R=(r_{ik})_{n\times n}$ using Equation (2.13) is obtained.
Step 6: The IF positive outranking flow $\tilde{\varphi}^{+}(x_i)$ and the intuitionistic fuzzy negative outranking flow $\tilde{\varphi}^{-}(x_i)$ by using Equation (2.15) and (2.15) are obtained.
Step 7: The relationship between $\tilde{\varphi}^{+}(x_i)$ and $\tilde{\varphi}^{-}(x_i)$ is determined. According to this relationship is made a ranking.

3. A Current Application of Intuitionistic Fuzzy PROMETHEE

The aim of this application; it is to create an algorithm that takes into account not only exam scores but also other factors affecting success of students. According to this algorithm, the factors affecting student achievement and exam scores have been evaluated together and the evaluation scores of the students have been calculated with the intuitionistic fuzzy PROMETHEE method. Each school points has been calculated depending on student examination score. While investigating the factors affecting the success, interviews were made with experts in the field and the resources related to this field were examined. As a result of these researches, interviews were made with school guidance teacher. In this process, the results of the exams applied to the students at school and private courses were examined. In addition, the method of individual interview was used to evaluate other factors affecting exam success. During the individual interview, the guidance teachers gave points to the students according to some criteria. Some of the interview questions asked are sub criteria, some are basic criteria. The weights of the criteria were determined in line with expert opinion. The basic lessons in the exam for students are Mathematics, Science, Social and Turkish. Other factors that affect success are; the economic situation of the family, the health status of the student, the study order of the student, the study discipline, the student's self-confidence, his relationship with his friends, his relationship with his family, and his private working environment. The guidance teachers were asked to give points in the range of 0-10 to these criteria for each student. The success of the students for each course was determined according to the points of the exam that the students took regularly every month. Afterwards, an evaluation score was calculated for each student by considering all the lessons and factors at the same time. As a result of this evaluation score, the success graph of the students was obtained and the success ranking was made. The personal information form have been prepared for the students and have been filled out with the support of guidance teacher for each student.
The set of criteria is as follows:

- K_1 :Turkish
- K_2 :Social
- K_3 :Mathematics
- K_4 :Science
- K_5 :Family factor- relationship to family
- K_6 :Study factor
  - Study system of the student
  - Study discipline
  - Private study environment
- K_7 :Self-confidence factor
  - Student's self-confidence
  - Relationship with friends, sociability
- K_8 :Demographic factors
  - Economic status of the family
- K_9 :Other factors
  - Health status of the student
  - Socio Cultural factors

Step 1: $\{A_1,A_2,A_3,A_4,A_5,A_6,A_7,A_8,A_9,A_{10},A_{11},A_{12},A_{13},A_{14},A_{15}\}$ be set of alternatives (students).
$\{K_1,K_2,K_3,K_4,K_5,K_6,K_7,K_8,K_9\}$ be set of criteria. Table 1 was created according to the net numbers of the students according to the results of the trial exams they took and the personal information forms filled in by the guidance teacher:

	C_1	C_2	C_3	C_4	C_5	C_6	C_7	C_8	C_9
A_1	23.5	12	27	14	9	10	5.5	8	9
A_2	27.5	12	10.25	0	9	9.66	8.5	7	4
A_3	20.75	6.5	20.75	0	9	9	7	8	7
A_4	17.5	12.5	14.25	0	3	5.33	5.5	7	6
A_5	19.5	8.5	10.75	8.25	9	8.33	7.5	8.	9
A_6	19	0	21	5.25	4.	7.33	9	7	9
A_7	26.5	0	11	0	3	7.66	6.5	5	9
A_8	20	3.75	9.5	2	6	7	4	8	3
A_9	17	13	1	0	9	8.33	7.5	10	10
A_{10}	21	8.5	0	0	3	7	7.5	5	9
A_{11}	15	7	1.75	0	9	9.33	8.5	7	10
A_{12}	9.25	5.25	0	0	9	9.33	8	8	10
A_{13}	8.25	5.25	0	0	3.5	8	5.5	10	10
A_{14}	7	0.5	0	1	6	9	6	9	6
A_{15}	29	0.5	24.75	2	10	8.66	8.5	8	8

Table 1: Exam results of students

Step 2: The weights of the criteria were calculated with the help of controlled sets. Weights of criteria $\mu_{\tilde{w}_j}, \nu_{\tilde{w}_j}$ determined with 3.1 in Table 2 according to the following situations:

Weights	$\mu_{\tilde{w}_j}$	$\nu_{\tilde{w}_j}$
$\tilde{w}_1$	1	0
$\tilde{w}_2$	0.5015	0.3
$\tilde{w}_3$	1	0
$\tilde{w}_4$	0.5015	0.3
$\tilde{w}_5$	0.3	0.5015
$\tilde{w}_6$	0.1126	0.5015
$\tilde{w}_7$	0.15	0.5015
$\tilde{w}_8$	0.1126	0.5015
$\tilde{w}_9$	0.075	0.5015

Table 2: Weights of criteria

- The contribution rates of the courses in the exam are as follows: (% 80)
  - K_1 :Turkish: %33,33
  - K_2 :Social: %16,67
  - K_3 :Mathematics: %33,33
  - K_4 :Science: %16,67
- Contribution rates of other factors that affect success are as follows:(%20) (These contribution rates have been determined with the opinions of experts in their field.)
  - K_5 :Family factor- relationship to family: %40
  - K_6 :Study factor: %15
  - K_7 :Self-confidence factor: %20
  - K_8 :Demographic factors: %15
  - K_9 :Other factors: %10

Step 3: Deviation $d_j(x_i,x_k)$ for each criterion; V-shape was calculated using generalization criteria. For the V-shape generalization criterion, the q indifference threshold is 40 for the K_1 and K_3 criteria, 20 for the K_2 and K_4 criteria, 10 for the criteria K_5, K_6, K_7, K_8, K_9, and the absolute preference threshold is p, and is 0 for all criteria. This is the threshold set by the researcher or decision maker. Threshold calculations for each study may vary.

$$d_j(x_i,x_k) = c_j(x_i) - c_j(x_k)$$

$$\mu_{ik}^{(j)} = \begin{cases} 0, & d_j(x_i,x_k) \leq q \\ \frac{d_j(x_i,x_k)-q}{p-q}, & q < d_j(x_i,x_k) \leq p \\ 1, & d_j(x_i,x_k) > p \end{cases}$$

Step 4: The intuitionistic fuzzy preference matrices $R^{(j)} = (r_{ik}^{(j)})_{n\times n}$ are determined by benefitted from equation $\nu_{ik} = \mu_{ki}$ and $\nu_{ki} = \mu_{ik}$.
Step 5: Overall intuitionistic fuzzy preference relation $R = (r_{ik})_{n\times n}$ is created using Equation (2.15).

Step 6: The intuitionistic fuzzy positive outranking flows and intuitionistic fuzzy negative outranking flows are calculated using Equation (2.16), (2.17).
Step 7: The values are ranked in Table 3:

$\rho(\tilde{\varphi}^+(x_1)) =$	0.895408163	$\rho(\tilde{\varphi}^-(x_1)) =$	0.939320674
$\rho(\tilde{\varphi}^+(x_2)) =$	0.895408163	$\rho(\tilde{\varphi}^-(x_2)) =$	0.898759017
$\rho(\tilde{\varphi}^+(x_3)) =$	0.89541498	$\rho(\tilde{\varphi}^-(x_3)) =$	0.900289988
$\rho(\tilde{\varphi}^+(x_4)) =$	0.895547851	$\rho(\tilde{\varphi}^-(x_4)) =$	0.895508379
$\rho(\tilde{\varphi}^+(x_5)) =$	0.895424014	$\rho(\tilde{\varphi}^-(x_5)) =$	0.898117312
$\rho(\tilde{\varphi}^+(x_6)) =$	0.895418008	$\rho(\tilde{\varphi}^-(x_6)) =$	0.895566097
$\rho(\tilde{\varphi}^+(x_7)) =$	0.895700692	$\rho(\tilde{\varphi}^-(x_7)) =$	0.895439819
$\rho(\tilde{\varphi}^+(x_8)) =$	0.896767967	$\rho(\tilde{\varphi}^-(x_8)) =$	0.895470838
$\rho(\tilde{\varphi}^+(x_9)) =$	0.895709231	$\rho(\tilde{\varphi}^-(x_9)) =$	0.895446384
$\rho(\tilde{\varphi}^+(x_{10})) =$	0.899104761	$\rho(\tilde{\varphi}^-(x_{10})) =$	0.895412326
$\rho(\tilde{\varphi}^+(x_{11})) =$	0.898075022	$\rho(\tilde{\varphi}^-(x_{11})) =$	0.895419782
$\rho(\tilde{\varphi}^+(x_{12})) =$	0.903031948	$\rho(\tilde{\varphi}^-(x_{12})) =$	0.89540828
$\rho(\tilde{\varphi}^+(x_{13})) =$	0.921333364	$\rho(\tilde{\varphi}^-(x_{13})) =$	0.895408168
$\rho(\tilde{\varphi}^+(x_{14})) =$	0.927293663	$\rho(\tilde{\varphi}^-(x_{14})) =$	0.895408162
$\rho(\tilde{\varphi}^+(x_{15})) =$	0.895408181	$\rho(\tilde{\varphi}^-(x_{15})) =$	0.89873238

Table 3: The intuitionistic fuzzy positive and negative outranking flows

The graphs of the alternatives in the positive, negative and net outranking flow are shown in Graph 1, Graph 2, Graph 3:

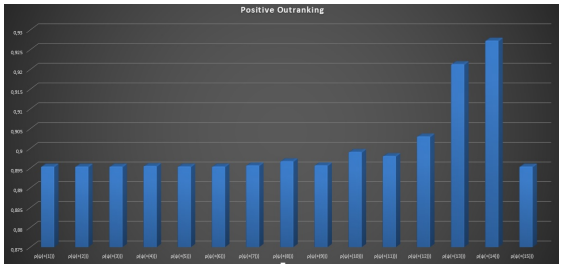

Figure 3.1: Graph of positive outranking flow

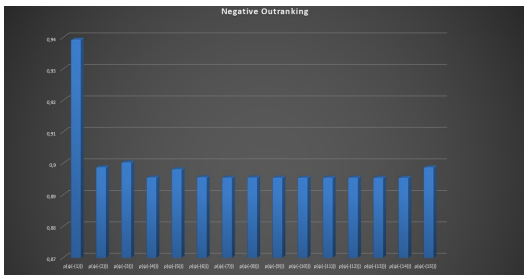

Figure 3.2: Graph of negative outranking flow

When the graphs are investigated, the ranking obtained between alternatives is as follows:

- Positive ranking:
  A_1, A_2, A_{15}, A_3, A_6, A_5, A_4, A_7, A_9, A_8, A_{11}, A_{10}, A_{12}, A_{13}, A_{14}
- Negative ranking:
  A_{14}, A_{13}, A_{12}, A_{10}, A_{11}, A_7, A_9, A_8, A_4, A_6, A_5, A_{15}, A_2, A_3, A_1

- According to these rankings, the students whose order is changed positively and negatively are A_{15},A_2,A_3,A_6,A_5,A_7,A_8 students. When the scores of these students according to the criteria are examined, the following judgments can be reached:
  - When all the criteria of these students were examined one by one, it was seen that the scores of some criteria were very low. In a positive sense, although we see a successful picture in general, the low scores of some criteria have attracted these students to the front ranks negatively.
  - According to the data obtained in this study; It has been observed that ranking only positively while making the decision process can lead to wrong results.
  - The method that allows us to make the right decision is the method that takes into account both positive and negative ranking at the same time.

In order to make a general ranking, a net outranking is needed since positive outranking and negative outranking are not the same. The net outranking flow in Table 4 is calculated with the help of the equation (2.18) and its graph is as follows:

$\rho(\tilde{\varphi}(x_1)) =$	-0.043912511
$\rho(\tilde{\varphi}(x_2)) =$	-0.003350854
$\rho(\tilde{\varphi}(x_3)) =$	-0.004875008
$\rho(\tilde{\varphi}(x_4)) =$	0.0000394712
$\rho(\tilde{\varphi}(x_5)) =$	-0.002693298
$\rho(\tilde{\varphi}(x_6)) =$	-0.000148089
$\rho(\tilde{\varphi}(x_7)) =$	0.000260873
$\rho(\tilde{\varphi}(x_8)) =$	0.001297128
$\rho(\tilde{\varphi}(x_9)) =$	0.000262847
$\rho(\tilde{\varphi}(x_{10})) =$	0.003692435
$\rho(\tilde{\varphi}(x_{11})) =$	0.00265524
$\rho(\tilde{\varphi}(x_{12})) =$	0.007623668
$\rho(\tilde{\varphi}(x_{13})) =$	0.025925196
$\rho(\tilde{\varphi}(x_{14})) =$	0.031885501
$\rho(\tilde{\varphi}(x_{15})) =$	-0.003324199

Table 4: Values of net outranking flow

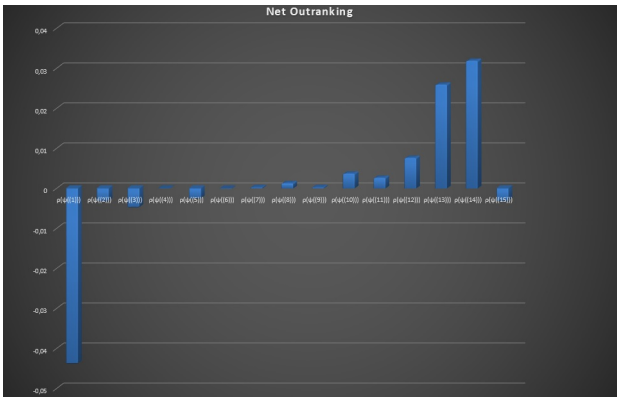

Figure 3.3: Graph of net outranking flow

As a result, the ranking from the best alternative to the worst alternative is as follows:

$$A_1, A_3, A_2, A_{15}, A_5, A_6, A_4, A_7, A_9, A_8, A_{11}, A_{10}, A_{12}, A_{13}, A_{14}$$

With net ranking, only the difference between positive and negative rankings is clearly visible. When choosing, ranking and evaluating, not only positive sense but also positive and negative sense alternatives are compared and a net ranking is obtained, the most accurate result is achieved. The ranking of the students was made, starting with the most successful according to the net ranking.

4. Conclusion

In this study, it is aimed to find the most rational solution to evaluate the youth of a country in education. Thanks to the method have been created an evaluation system that takes into account not only the exam scores of the students, but also other factors that affect the success of the students. In our previous studies, we developed and analyzed different methods that calculate students' success based on exam scores. One of the deficiencies we see while evaluating in education is that evaluation is made only according to the exam results. Based on these reasons, an intuitionistic fuzzy logic-based evaluation system was created for the first time in education with this method, which will add an innovation to the education system. More objective and rational results will be obtained thanks to this new method that we present to the evaluation system in education. The general algorithm is detailed to show the applicability of this new method in all areas. This algorithm can be applied in any situation where it is desired to be preferred among multi-criteria alternatives. New research can be done by following the steps in the algorithm given in this study. This study will lead to innovations not only in the field of education but also in many applications. Thanks to this system that we will create that will have the ability to apply not only in the field of education, but also in many fields, many factors will be evaluated at the same time and different degrees of importance will be determined for each factor.
Intuitionistic fuzzy PROMETHEE is a method that attracts our attention thanks to its benefits such as allowing the researcher to observe the positive and negative rankings simultaneously, expressing the degree of hesitation, changing the significance weights of the criteria, and using different methods when identifying the significance levels for each criterion, putting the degree of hesitation of significance weights into action, and enabling decision-makers, who are given the opportunity to use different criteria types and different criteria types for alternatives and criteria, to establish a unique system; moreover, the method also provides us numerous advantages while using it in our application area. Because of these advantages, the intuitionistic fuzzy PROMETHEE method continues to be applied in many decision-making processes.
In the last part of our study, our method is explained, visualized and interpreted with graphics. Factors affecting student achievement and

exam scores were evaluated together with the intuitive fuzzy PROMETHEE method and the evaluation scores of the students were calculated with the determined algorithm. The accuracy, suitability and rationality of the developed method has been proven with the given application. This method will provide rational, useful, profitable results in many areas and will facilitate the work of many decision makers. Thanks to our work, we shed light on many areas where our method will be applied.

Acknowledgements

The authors would like to express their sincere thanks to the editor and the anonymous reviewers for their helpful comments and suggestions.

Funding

There is no funding for this work.

Availability of data and materials

Not applicable.

Competing interests

The authors declare that they have no competing interests.

Author's contributions

All authors contributed equally to the writing of this paper. All authors read and approved the final manuscript.

References

[1] L. A. Zadeh, *Fuzzy sets* Information and Control, **8** (1965) 338-353.
[2] K. Atanassov, *Intuitionistic fuzzy sets* Fuzzy Sets Syst., **20**(1) (1986), 87-96.
[3] K. Atanassov, *More on intuitionistic fuzzy sets*, Fuzzy Sets Syst., **33**(1) (1989), 37-45.
[4] M. Majumder, *Multi Criteria Decision Making*, Chapter 2, Springer, (2015), 35-47.
[5] J. P. Brans, Lingenierie de la decision; Elaboration dinstruments daidealadecision, Lamethode PROMETHEE, in: R. Nadeau, M. Landry, ed., Laidea la Decision: Nature, Instruments et Perspectives d Avenir, Quebec, Canada, Presses de lUniversite Laval, (1982), 183-213.
[6] G. Büyüközkan, F. Göçer, *Application of a new combined intuitionistic fuzzy MCDM approach based on axiomatic design methodology for the supplier selection problem*, Appl. Soft Comput., **52** (2017), 1222-1238.
[7] A. Albadvi, *Formulating national information technology strategies: A preference ranking model using PROMETHEE method*, Eur. J. Oper. Res., **153** (2004), 290-296.
[8] A. Albadvi, S. K. Chaharsooghi, A. Esfahanipour, *Decision making in stock trading: An application of PROMETHEE*, Eur. J. Oper. Res., **177** (2007) 673-683.
[9] M. Behzadian, R. B. Kazemzadeh, A. Albadvi, M. Aghdasi, *PROMETHEE: A comprehensive literature reviewon methodologies and applications*, Eur. J. Oper. Res., **200** (2010), 198-215.
[10] J. P. Brans, B. Mareschal, P. Vincke, *PROMETHEE: a new family of outranking methods in multicriteria analysis*, Oper. Res., IFORS **84** (1984), 477-490.
[11] N. Halouani, H. Chabchoub, J. M. Martel, *PROMETHEEMD-2T method for project selection*, Eur. J. Oper. Res., **195** (2009), 841-849.
[12] R. Krishankumar, K. S. Ravichandran, A. B. Saeid, *A new extension to PROMETHEE under intuitionistic fuzzy environment for solving supplier selection problem with linguistic preferences*, Appl. Soft Comput., **60** (2017), 564-576.
[13] K. J. Zhang, C. Kluck, G. Achari, *A comparative approach for ranking contaminated sites based on the risk assessment paradigm using fuzzy PROMETHEE*, Environ Manage., **44** (2009), 952-967.
[14] F. Tuğrul, M. Çitil, Evaluating the factors affecting success of students with the intuitionistic fuzzy PROMETHEE method, 3rd International Conference on Pure and Applied Mathematics, Van, Turkey, 2020.
[15] F. Tuğrul, M. Çitil, *A new perspective on evaluation system in education with intuitionistic fuzzy logic and PROMETHEE algorithm*, Journal of Universal Mathematics, **4**(1) (2021), 13-24.
[16] F. Tuğrul, *Application of intuitionistic fuzzy logic with a new method in multi criteria decision making process*, Ph.D. Thesis. Kahramanmaraş Sütçü İmam University, 2021.
[17] Z. S. Xu, *Intuitionistic fuzzy aggregation operators*, IEEE Trans. Fuzzy Syst., **15** (2007), 1179-1187.
[18] Z. S. Xu, R. R. Yager, *Some geometric aggregation operators based on intuitionistic fuzzy set*, Int. J. Gen. Syst., **35** (2006), 417-433.
[19] E. Szmidt, J. Kacprzyk, Amount of information and its reliability in the ranking of Atanassov's intuitionistic fuzzy alternatives, in: E. Rakus-Andersson, R.R. Yager, N. Ichalkaranje, L. Jain, ed. Recent Advances in Decision Making (Studies in Computational Intelligence), Berlin, Germany, Springer, (2009), 7-19.
[20] H. C. Liao, Z. S. Xu, *Priorities of intuitionistic fuzzy preference relation based on multiplicative consistency*, IEEE Trans. Fuzzy Syst., **22**(6) (2014), 1669-1681.
[21] G. Çuvalcıoğlu, *Some properties of controlled set theory*, Notes on Intuitionistic Fuzzy Set, **20**(2) (2014) 37-42.
[22] G. Çuvalcıoğlu, *Controlled set theory*, Bogolyubov Readings, DIF-2013, Ukraine, **342** (2013).
[23] H. C. Liao, Z. S. Xu, *Some algorithms for group decision making with intuitionistic fuzzy preference information*, International Journal of Uncertainty Fuzziness and Knowledge-Based Systems, **22**(4) (2014), 505-529.
[24] Z. J. Wang, *Derivation of intuitionistic fuzzy weights based on intuitionistic fuzzy preference relations*, Appl. Math. Model., **37** (2013), 6377-6388.
[25] Z. S. Xu, H. C. Liao, *Intuitionistic fuzzy analytic hierarchy process*, IEEE Trans. Fuzzy Syst., **22**(4) (2014), 749-761.
[26] P. H. Vincke, J. P. Brans, *A preference ranking organization method: (The PROMETHEE Method for Multiple Criteria Decision-Making)*, Manag. Sci., **31**(6) (1985), 647-656.
[27] Z. S. Xu, *Intuitionistic preference relations and their application in group decision making*, Information Sciences, **177**(11) (2007), 2363-2379.
[28] H. Liao, Z. S. Xu, *Multi-criteria decision making with intuitionistic fuzzy PROMETHEE*, J. Intell. Fuzzy Syst., **27** (2014), 1703-1717.

Journal of Mathematical Sciences and Modelling, 5 (2) (2022) 57-62
Research Article

Journal of Mathematical Sciences and Modelling

Journal Homepage: www.dergipark.gov.tr/jmsm
ISSN 2636-8692
DOI: http://dx.doi.org/10.33187/jmsm.1149614

New Travelling Wave Solutions of Conformable Cahn-Hilliard Equation

Esin Aksoy[1*] **and Adem Cengiz Çevikel**[1]

[1]*Department of Mathematics, Faculty of Science and Arts, Yildiz Tehcnical University, Istanbul, Turkey*
[*]*Corresponding author*

Article Info

Keywords: *Conformable derivatives, Exact solution, Nonlinear water waves, Travelling wave solutions*
2010 AMS: *35C05, 35L05, 35R11*
Received: *27 July 2022*
Accepted: *15 August 2022*
Available online: *30 August 2022*

Abstract

In this article, two methods are proposed to solve the fractional Cahn-Hilliard equation. This model describes the process of phase separation with nonlocal memory effects. Cahn-Hilliard equations have numerous applications in real-world scenarios, e.g., material sciences, cell biology, and image processing. Different types of solutions have been obtained. For this, the fractional complex transformation has been used to convert fractional differential equation to ordinary differential equation of integer order. As a result, these solutions are new solutions that do not exist in the literature.

1. Introduction

Shallow water areas show nonlinear effects during the propagation and transformation of swelling waves. Nonlinear equations such as Cahn-Hilliard equation exhibit significant spectral energy transfer for finite amplitude waves in shallow areas above the flat seafloor [1]. Chaotic oscillations usually occur in nonlinear dynamical systems (especially in watersheds). This systems can be represented by Cahn-Hilliard equation with nonlinear oscillations and external periodic excitation [2].
Fractional differential equations (FDEs) are generalizations of known differential equations (ODEs). Fractional order partial differential equations (fPDEs) are used effectively in many fields of science because they give more realistic results in modeling real life problems. [3–6]. Many useful methods have been presented for exact solutions of fPDEs as the $\left(\frac{G'}{G}\right)$-expansion [7–9], the sub-equation [10, 11], the exp-function [12–15], the first integral [16], the functional variable [17, 18], the modified simplest equation [19, 20]. The Kudryashov method [21]. With the help of these methods, solutions of fPDEs in many different forms are calculated.
In the next section, the extended tanh method and the sine-cosine method are introduced. In the next section, we will find the traveling wave solutions of the fractional Cahn-Hilliard equation (fCHE) via the this methods. We will talk about the data obtained in the last section.

2. Presentment of the Methods

2.1. The conformable derivative

The basic limit definition of this derivative is [22]:

$$D_t^{\alpha} f(t) = \begin{cases} \frac{1}{\Gamma(1-\alpha)} \frac{d}{dt} \int_0^t (t-\xi)^{-\alpha} (f(\xi) - f(0)) d\xi & , \quad 0 < \alpha < 1 \\ \\ (f^{(n)}(t))^{(\alpha-n)} & , \quad n \leq \alpha < n+1, \quad n \geq 1. \end{cases} \tag{2.1}$$

Some important properties of the conformable derivative were summarized in [23, 24]. Now, we briefly describe the definition and theorems of conformable derivatives:

***Email addresses and ORCID numbers*: eesinaksoy@gmail.com, 0000-0001-6386-4277 (E. Aksoy), acevikel@yildiz.edu.tr, 0000-0002-7359-3156 (A. C. Çeviker),**

Definition 2.1. *Let $g:(0,\infty)\to R$ be a function. The conformable derivative of g for order α is defined by*

$$T_\alpha(g(k))=\lim_{\varepsilon\to 0}\frac{g\left(k+\varepsilon k^{1-\alpha}\right)-g(k)}{\varepsilon} \tag{2.2}$$

for all $k>0,\quad \alpha\in(0,1)$.

Theorem 2.2. *If a function $g:[0,\infty)\to R$ is $\alpha-$differentiable at $t_0>0,\ \alpha\in(0,1],\ g$ is continuous at t_0.*

Theorem 2.3. *Let f and g be $\alpha-$differentiable at a point $t>0,\ \alpha\in(0,1]$:*

$$\begin{aligned}
&T_\alpha(\alpha f+bg)=aT_\alpha(f)+bT_\alpha(g),\quad \text{for all } a,b\in R.\\
&T_\alpha(t^p)=pt^{p-\alpha},\quad \text{for all } p\in R.\\
&T_\alpha(\lambda)=0,\quad \text{for all constant functions } f(t)=\lambda.\\
&T_\alpha(fg)=fT_\alpha(g)+gT_\alpha(f).\\
&T_\alpha\left(\frac{f}{g}\right)=\frac{gT_\alpha(f)-fT_\alpha(g)}{g^2}.
\end{aligned} \tag{2.3}$$

If g is differentiable:

$$T_\alpha(g)(t)=t^{1-\alpha}\frac{dg}{dt}(t). \tag{2.4}$$

A nonlinear conformable partial differential equations (CPDEs) with two independent variables are:

$$P\left(\frac{\partial^\alpha u}{\partial t^\alpha},\frac{\partial^\alpha u}{\partial x^\alpha},\frac{\partial^{2\alpha}u}{\partial t^{2\alpha}},\frac{\partial^{2\alpha}u}{\partial x^{2\alpha}},\ldots\right)=0,\quad 0<\alpha\le 1, \tag{2.5}$$

$$u(x,t)=U(\xi),\quad \xi=k\frac{x^\alpha}{\alpha}-c\frac{t^\alpha}{\alpha}, \tag{2.6}$$

$u(x,t)$ is a traveling wave solution and c is a constant and will be calculated later.

$$\frac{\partial^\alpha}{\partial t^\alpha}=-c\frac{\partial}{\partial\xi},\quad \frac{\partial^{2\alpha}}{\partial t^{2\alpha}}=c^2\frac{\partial^2}{\partial\xi^2},\quad \frac{\partial^\alpha u}{\partial x^\alpha}=k\frac{\partial}{\partial\xi},\quad \frac{\partial^{2\alpha}u}{\partial x^{2\alpha}}=k^2\frac{\partial^2}{\partial\xi^2},\ldots$$

using equation (2.6), nonlinear CPDE equation (2.5) can be reduced to a nonlinear ODE equation (2.7):

$$Q(U,U',U'',U''',\ldots)=0. \tag{2.7}$$

where the prime denotes the derivation with respect to ξ.

2.2. The extended $\tanh-\coth$ method

In [25], this method is summarized as follows:
From the Y independent variable and its derivatives:

$$Y=\tanh(\xi)\quad \text{or}\quad Y=\coth(\xi), \tag{2.8}$$

$$\begin{aligned}
\frac{d}{d\xi} &= \left(1-Y^2\right)\frac{d}{dY},\\
\frac{d^2}{d\xi^2} &= \left(1-Y^2\right)\left(-2Y\frac{d}{dY}+\left(1-Y^2\right)\frac{d^2}{dY^2}\right).
\end{aligned} \tag{2.9}$$

The $\tanh-\coth$ method:

$$U(\xi)=S(Y)=\sum_{k=0}^{m}a_kY^k, \tag{2.10}$$

where $a_k(k=0,1,2,\ldots,m)$ are constants.
Equation (2.10) can be expanded as follows [26].

$$U(\xi)=S(Y)=\sum_{k=0}^{m}a_kY^k+\sum_{k=1}^{m}b_kY^{-k}, \tag{2.11}$$

where $a_k(k=0,1,2,\ldots,m)$, $b_k(k=0,1,2,\ldots,m)$ are constants. The positive integer m can be determined by considering the homogeneous balance between the highest order derivatives and the nonlinear terms appearing in equation (2.7).

2.3. The sine-cosine method

In [27], this method is summarized as follows:
The solutions of nonlinear equations is

$$u(x,t)=\left\{\begin{array}{ll}\lambda\sin^{\beta}(\mu\xi), & |\xi|\leq\frac{\pi}{\mu},\\ 0, & \text{otherwise}\end{array}\right\}, \tag{2.12}$$

$$u(x,t)=\left\{\begin{array}{ll}\lambda\cos^{\beta}(\mu\xi), & |\xi|\leq\frac{\pi}{2\mu},\\ 0, & \text{otherwise}\end{array}\right\} \tag{2.13}$$

where λ,μ and β are parameters to be calculated. μ and c in wave transform are the wave number and the wave speed.
From equation (2.12):

$$\begin{aligned}&u(\xi)=\lambda\sin^{\beta}(\mu\xi),\\ &u^{n}(\xi)=\lambda^{n}sin^{n\beta}(\mu\xi),\\ &(u^{n})_{\xi}=n\mu\beta\lambda^{n}cos(\mu\xi)sin^{n\beta-1}(\mu\xi),\\ &(u^{n})_{\xi\xi}=-n^{2}\mu^{2}\beta^{2}\lambda^{n}sin^{n\beta}(\mu\xi)+n\mu^{2}\lambda^{n}\beta(n\beta-1)sin^{n\beta-2}(\mu\xi),\end{aligned} \tag{2.14}$$

and from equation (2.13):

$$\begin{aligned}&u(\xi)=\lambda\cos^{\beta}(\mu\xi),\\ &u^{n}(\xi)=\lambda^{n}\cos^{n\beta}(\mu\xi),\\ &(u^{n})_{\xi}=-n\mu\beta\lambda^{n}\sin(\mu\xi)\cos^{n\beta-1}(\mu\xi),\\ &(u^{n})_{\xi\xi}=-n^{2}\mu^{2}\beta^{2}\lambda^{n}\cos^{n\beta}(\mu\xi)+n\mu^{2}\lambda^{n}\beta(n\beta-1)\cos n^{n\beta-2}(\mu\xi).\end{aligned} \tag{2.15}$$

We substitute equation (2.15) or (2.14) in the reduced equation (2.7). We can sum all terms with the same power in $cos^{k}(\mu\xi)$ or $sin^{k}(\mu\xi)$ and set their coefficients to zero to get a system of algebraic equations. So, we can get all values of parameters μ,β and λ.

3. Applications

Let us investigate traveling wave solutions of space-time fCHE in order to demonstrate the effectiveness of the methods.

3.1. Exact solutions of the fCHE

3.1.1. The extended tanh method

Now we will investigate the solutions of equation (3.1) with the extended tanh method. We will then interpret the results obtained.

$$\frac{\partial^{\alpha}u}{\partial t^{\alpha}}-r\frac{\partial^{\alpha}u}{\partial x^{\alpha}}-6u\left(\frac{\partial^{\alpha}u}{\partial x^{\alpha}}\right)^{2}-\left(3u^{2}-1\right)\frac{\partial^{2\alpha}u}{\partial x^{2\alpha}}+\frac{\partial^{4\alpha}u}{\partial x^{4\alpha}}=0,\quad 0<\alpha\leq 1, \tag{3.1}$$

nonlinear wave equation. We have applied intended tanh method on the Conformable CHE for gaining the exact solutions:

$$u(x,t)=U(\xi),\quad \xi=k\frac{x^{\alpha}}{\alpha}-c\frac{t^{\alpha}}{\alpha}.$$

Equation (3.1) can be reduced to equation (3.2):

$$-cU-krU-3k^{2}U^{2}U'+k^{2}U'+k^{4}U'''=0, \tag{3.2}$$

c,r and k are constants.
Balancing U''' with $U^{2}U'$ yields $m=1$. So, the solution of equation is equation (3.3) format.

$$U(\xi)=a_{0}+a_{1}Y+b_{1}Y^{-1},\quad Y=\tanh(\xi),\quad Y'=1-Y^{2}. \tag{3.3}$$

Here a_0, a_1, b_1, k and c are constants such that $a_1 \neq 0$. Substituting equation (3.3) into equation (3.2), collecting the coefficients of Y^i $(i = -4, ...4)$ and set it to zero we obtain the system

$$\begin{aligned}
3a_1^3k^2 - 6a_1k^4 &= 0,\\
6a_0a_1^2k^2 &= 0,\\
3a_0^2a_1k^2 - 3a_1^3k^2 + 3a_1^2b_1k^2 + 8a_1k^4 - a_1k^2 &= 0,\\
6a_0a_1^2k^2 - a_1kr - a_1c &= 0,\\
(a_1+b_1)(k^2 - 2k^4 - 3a_0^2k^2 - 3k^2a_1b_1) - a_0(kr+c) &= 0,\\
6a_0b_1^2k^2 - b_1kr - b_1c &= 0,\\
3a_0^2b_1k^2 + 3a_1b_1^2k^2 - 3b_1^3k^2 + 8b_1k^4 - b_1k^2 &= 0,\\
6a_0b_1^2k^2 &= 0,\\
3b_1^3k^2 - 6b_1k^4 &= 0.
\end{aligned} \tag{3.4}$$

The exact solutions obtained from this system of equations are:

$$\begin{aligned}
u_1(x,t) &= \frac{1}{\tanh\left(\pm\frac{\sqrt{2}}{2}x^\alpha \pm \frac{\sqrt{2}}{2}rt^\alpha\right)},\\
u_2(x,t) &= -\frac{1}{\tanh\left(\pm\frac{\sqrt{2}}{4}x^\alpha \pm \frac{\sqrt{2}}{4}rt^\alpha\right)},\\
u_3(x,t) &= \tanh\left(\pm\frac{\sqrt{2}}{2}x^\alpha \pm \frac{\sqrt{2}}{2}rt^\alpha\right),\\
u_4(x,t) &= -\tanh\left(\pm\frac{\sqrt{2}}{4}x^\alpha \pm \frac{\sqrt{2}}{4}rt^\alpha\right),\\
u_5(x,t) &= \pm\frac{1}{2}\tanh\left(\pm\frac{\sqrt{2}}{4}x^\alpha \pm \frac{\sqrt{2}}{4}rt^\alpha\right) \pm \frac{1}{2\tanh\left(\pm\frac{\sqrt{2}}{4}x^\alpha \pm \frac{\sqrt{2}}{4}rt^\alpha\right)},\\
u_6(x,t) &= \pm\frac{i\sqrt{2}}{2}\tanh\left(\pm\frac{i}{2}x^\alpha \pm \frac{i}{2}rt^\alpha\right) \pm \frac{1}{2}\frac{i\sqrt{2}}{\tanh\left(\pm\frac{i}{2}x^\alpha \pm \frac{i}{2}rt^\alpha\right)},
\end{aligned} \tag{3.5}$$

where r is arbitrary constant.

3.1.2. The sine-cosine method

Now we will investigate the solutions of equation (3.1) with this method. We will then interpret the results obtained. We have applied the method on the Conformable CHE for gaining the exact solutions. Using the ξ wave transform, equation (3.1) can be reduced to equation (3.6):

$$-cU - krU - 3k^2U^2U' + k^2U' + k^4U''' + q = 0, \tag{3.6}$$

c, r and k are constants, q is a constant of integration.
Balancing U''' with U^2U' yields $m = 1$. So, the solution of equation is equation (3.7) or equation (3.8) format:

$$u(x,t) = \lambda\cos^\beta(\mu\xi), \tag{3.7}$$

$$u(x,t) = \lambda\sin^\beta(\mu\xi). \tag{3.8}$$

We substitute equation (3.7) into the reduced equation obtained from equation (3.6).

$$\begin{aligned}
\frac{(-k^2\lambda\mu + 11k^4\lambda^3\mu^3 + qsin(\mu\xi))}{sin(\mu\xi)} &= 0,\\
\frac{(-c\lambda sin(\mu\xi) - kr\lambda sin(\mu\xi))}{sin(\mu\xi)} &= 0,\\
\frac{(-12\lambda\mu^3k^4 + 3\lambda^3\mu k^2 + a_1\mu k^2)}{sin(\mu\xi)} &= 0,\\
\frac{(6\lambda\mu^3k^4 - 3\lambda^3\mu k^2)}{sin(\mu\xi)} &= 0.
\end{aligned} \tag{3.9}$$

After the necessary arrangements have been made the following exact solutions obtained:

$$u_{7,8}(x,t) = \frac{\sqrt{3}}{3}\cos^{-1}\left(\pm\frac{r^2}{6c}\left(\frac{-1}{r}x^\alpha - t^\alpha\right)\right). \tag{3.10}$$

where r and c are arbitrary constants.

4. Conclusion

In this paper we have been successfully obtained traveling wave solutions of the fractional Cahn-Hilliard equation. Many of the results obtained are new solutions that do not exist in the literature. This hyperbolic solutions are significant for the explanation of many physical phenomena, ocean engineering and science. This implies that the methods are more powerful and effective in finding the exact solutions of nonlinear fractional differential equations. Many new solutions can be found with this methods. Using this methods possible to solve other similar nonlinear equations and systems of equations. The obtained solutions in this research have been found by aid of Maple packet program.

Acknowledgments

The authors would like to express their sincere thanks to the editor and the anonymous reviewers for their helpful comments and suggestions.

Funding

There is no funding for this work.

Availability of data and materials

Not applicable.

Competing interests

The authors declare that they have no competing interests.

Author's contributions

All authors contributed equally to the writing of this paper. All authors read and approved the final manuscript.

References

[1] G. I. Dolgikha, D. P. Kovalevb, P. D. Kovalevb, *Excitation of Under-ice seiches of a sea port of the sea of Okhotsk*, Doklady Earth Sciences, **486**(2) (2019), 651–653.
[2] I. Kovacic, M. J. Brennan, *The Duffing Equation: Nonlinear Oscillators and Their Behavior*, John Wiley and Sons, London, 2011.
[3] K.S. Miller, B. Ross, *An introduction to the Fractional Calculus and Fractional Differential Equations*, Wiley, New York, 1993.
[4] I. Podlubny, *Fractional Differential Equations*, Academic Press, California, 1999.
[5] R. Hilfer, *Applications of Fractional Calculus in Physics*, World Scientific Publishing, River Edge, NJ, USA; 2000.
[6] A. A. Kilbas, H. M. Srivastava, J. J. Trujillo, *Theory and Applications of Fractional Differential Equations*, Elsevier, Amsterdam, 2006.
[7] A. Bekir, O. Güner, B. Ayhan, A. C. Çevikel, *Exact solutions for fractional differential-difference equations by (G'/G)-expansion method with modified Riemann-Liouville derivative, Advances in Applied Mathematics and Mechanics*, **8**(2) (2016), 293–305.
[8] O. Güner, E. Aksoy, A. Bekir, A. C. Çevikel, *Different methods for $(3+1)$-dimensional space-time fractional modified KdV-Zakharov-Kuznetsov equation*, Comput. Math. with Appl., **71** (2016), 1259–1269.
[9] O. Guner, A. Bekir, A. C. Çevikel, *A variety of exact solutions for the time fractional Cahn-Allen equation*, European Physical Journal Plus, **130**(2015), 146.
[10] E. Aksoy, A. C. Çevikel, A. Bekir, *Soliton solutions of $(2+1)$-dimensional time-fractional Zoomeron equation*, Optik, **127**(17) (2016), 6933–6942.
[11] A. Bekir, E. Aksoy, A. C. Çevikel, *Exact solutions of nonlinear time fractional partial differential equations by sub-equation method*, Math. Methods Appl. Sci., **38**(13) (2015), 2779–2784.
[12] A. Bekir, O. Güner, A. C. Cevikel, *Fractional complex transform and exp-function methods for fractional differential equations*, Abstr. Appl. Anal., **2013** (2013), Article ID: 426462, 8 pages.
[13] O. Güner, A. C. Çevikel, *A procedure to construct exact solutions of nonlinear fractional differential equations*, Sci. World J., **2014** (2014), 489495.

[14] A. C. Çevikel, *New exact solutions of the space-time fractional KdV-Burgers and non-linear fractional Foam Drainage equation*, Therm. Sci., **22** (2018), 15–24.
[15] A. Bekir, O. Güner, A. C. Çevikel, *The Exp-function method for some time-fractional differential equations*, IEEE/CAA J. Autom. Sin., **4** (2017), 315–321.
[16] E. Aksoy, A. Bekir, A. C. Çevikel, *Study on fractional differential equations with modified Riemann-Liouville derivative via Kudryashov method*, Int. J. Nonlinear Sci. Numer. Simul., **20**(5) (2019), 511–516.
[17] H. Rezazadeh, J. Vahidi, A. Zafar, A. Bekir, *The functional variable method to find new exact solutions of the nonlinear evolution equations with dual-power-law nonlinearity*, Int. J. Nonlinear Sci. Numer. Simul., **21**(3-4) (2020), 249-257.
[18] A. C. Çevikel, A. Bekir, M. Akar, S. San, *Procedure to construct exact solutions of nonlinear evolution equation*s, Pramana Journal of Physics, **79**(3) (2012), 337–344.
[19] N. Taghizadeh, M. Mirzazadeh, M. Rahimian, M. Akbari, *Application of the simplest equation method to some time-fractional partial differential equations*, Ain Shams Eng., **4** (2013), 897–902.
[20] N. Savaissou, B. Gambo, H. Rezazadeh, A. Bekir, S. Y. Doka, *Exact optical solitons to the perturbed nonlinear Schrodinger equation with dual-power law of nonlinearity*, Opt. Quantum Electron., **52** (2020), 318.
[21] A. C. Çevikel, E. Aksoy, *Soliton solutions of nonlinear fractional differential equations with their applications in mathematical physics*, Revista Mexicana de Fisica, **67**, (3) (2021), 422–428.
[22] R. Khalil, M. Al Horani, A. Yousef, M. Sababheh, *A new definition of fractional derivative*, J. Comput. Appl. Math., **264** (2014), 65–70.
[23] T. Abdeljawad, *On conformable fractional calculus*, J. Comput. Appl. Math., **279** (2015), 57–66.
[24] M. Eslami, H. Rezazadeh, *The first integral method for Wu–Zhang system with conformable time-fractional derivative*, Calcolo, **53** (2016), 475–485.
[25] A. C. Çevikel, A. Bekir, *New solitons and periodic solutions for* $(2+1)$*-dimensional Davey-Stewartson equations*, Chinese J. Phys., **51**(1) (2013), 1–13.
[26] A. Bekir, A. C. Çevikel, *Solitary wave solutions of two nonlinear physical models by* $\tanh-\coth$ *method*, Communications in Commun. Nonlinear Sci. Numer. Simul., **14**(5) (2009), 1804–1809.
[27] A. Bekir, A. C. Çevikel, *New solitons and periodic solutions for nonlinear physical models in mathematical physics*, Nonlinear Anal. Real World Appl., **11**(4) (2010), 3275–3285.
[28] H. Jafari, H. Tajadodi, D. Baleanu, A. A. Al-Zahrani, Y. A. Alhamed, A. H. Zahid, *Fractional sub-equation method for the fractional generalized reaction Duffing model and nonlinear fractional Sharma-Tasso-Olver equation*, Cent. Eur. J. Phys., **11**(10) (2013), 1482–1486.

Journal of Mathematical Sciences and Modelling, 5 (2) (2022) 63-66
Research Article

Journal of Mathematical Sciences and Modelling

Journal Homepage: www.dergipark.gov.tr/jmsm
ISSN 2636-8692
DOI: http://dx.doi.org/10.33187/jmsm.1058501

A Short Proof of the Size of Edge-Extremal Chordal Graphs

Mordechai Shalom

Department of Computer Engineering. Işık University, Istanbul, Turkey

Article Info

Keywords: *Chordal graphs, Edge-extremal graphs, Matching number*
2010 AMS: *05C35, 05C62*
Received: *16 January 2022*
Accepted: *19 March 2022*
Available online: *30 August 2022*

Abstract

Blair et. al. [3] have recently determined the maximum number of edges of a chordal graph with a maximum degree less than d and the matching number at most ν by exhibiting a family of chordal graphs achieving this bound. We provide simple proof of their result.

1. Introduction

Consider a graph $G=(V,E)$ with maximum degree $\Delta(G)<d$ and matching number ν. Vizing's theorem states that there exists a coloring of E using at most $\Delta(G)+1\leq d$ colors. Each color class contains at most ν edges, since it constitutes a matching. Therefore, G has at most $d\cdot\nu$ edges, i.e., bounding both the matching number and the maximum degree of a graph bounds the number of its edges. We want to note that none of the parameters d and ν alone is sufficient to bound the number of edges of G, as the following examples show. The graph mK_2 that is a matching with m vertices has maximum degree 1 and an unbounded number of edges. On the other hand, the graph $K_{1,m}$ which is a star with m leaves has matching number 1 and an unbounded number of edges.
This observation gives rise to the following two questions

- What is the maximum number $m(d,\nu)$ of edges of a graph with matching number at most ν and maximum degree less than d?
- What is the set $\mathscr{M}(d,\nu)$ graphs with maximum degree less than d and matching number at most ν that contain (exactly) $m(d,\nu)$ edges ?

The first question is resolved in the work [1] and the second is resolved later in the work [2] that provided a constructive proof.
The same questions can be posed by confining ourselves to any graph class $\mathscr{C}$, therefore defining:

- $m_{\mathscr{C}}(d,\nu)$ as the maximum number of edges of a graph $G\in\mathscr{C}$ with maximum degree $\Delta(G)<d$ and matching number at most ν, and
- $\mathscr{M}_{\mathscr{C}}(d,\nu)$ the set of graphs $G\in\mathscr{C}$ with maximum degree $\Delta(G)<d$, matching number at most ν having $m_{\mathscr{C}}(d,\nu)$ edges.

A graph $G\in\mathscr{M}(d,\nu)$ (resp. $G\in\mathscr{M}_{\mathscr{C}}(d,\nu)$) is said to be *edge-extremal* (resp. *edge-extremal-$\mathscr{C}$*).
The authors of [3] consider the class of chordal graphs, and determine the number $m_{\text{CHORDAL}}(d,\nu)$ by exhibiting a set of edge-extremal-chordal graphs. In this work we provide a short proof of their following result.

Theorem 3.3. *[3] There exists an edge-extremal graph in $\mathscr{M}_{\text{CHORDAL}}(d,\nu)$ that is a disjoint union of cliques and stars.*

The result is obtained by showing that all the minimal elements of a carefully chosen preorder on the set of minimal representations of the graphs in $\mathscr{M}_{\text{CHORDAL}}(d,\nu)$ have this property. Namely, they are disjoint unions of cliques and stars.

2. Preliminaries

A vertex v of a graph G is *simplicial* if its neighbourhood is a clique and *universal* if its closed neighbourhood is the entire graph. A *star* is a tree with at most one non-leaf vertex. A d-star is a star with maximum degree d. Any total order on a set A defines a corresponding *lexicographic* order on the set A^* of all sequences over the elements of A. In a way similar to a dictionary, the order between two distinct elements a,b of A^* in the lexicographic order is determined by the order of the entries $a_i,b_i\in A$ where i is the lowest index such that $a_i\neq b_i$.

***Email address and ORCID number*: cmshalom@gmail.com, 0000-0002-2688-5703 (M. Shalom)**

Observation 2.1. *A simplicial vertex of a graph G is of maximum degree if and only if G is a complete graph.*

A graph G is *factor-critical* if every subgraph obtained by the removal of a single vertex from G admits a perfect matching. It is easy to see that a factor-critical graph is odd and connected.

Definition 2.2. *A graph class $\mathscr{C}$ is* special hereditary *if*

- *$\mathscr{C}$ is closed under the vertex deletion and disjoint union operations, and*
- *$\mathscr{C}$ contains all stars and cliques.*

We will use the following theorem proven in [2].

Theorem 2.3. *[2] Let $\mathscr{C}$ be a special hereditary graph class. Let $G \in \mathscr{C}$ be an edge-extremal graph having the maximum possible number of connected components that are stars . Then every other connected component of G is factor-critical.*

Chordal graphs and subtree representations: A *hole* of a graph is an induced cycle of at least four vertices. A graph is *chordal* if it does not contain a hole.
Consider a forest T and a set $\mathscr{T} = \{T_1, \ldots, T_n\}$ of n subtrees of T. Without loss of generality we assume that every edge of T is used by at least one tree in $\mathscr{T}$. In other words, T is the union of the trees in $\mathscr{T}$. We denote by $G(\mathscr{T})$ *the intersection graph* of these subtrees, i.e., the graph with vertex set $[n] = \{1, 2, \ldots n\}$ such that two vertices $i, j \in [n]$ of G are adjacent if and only if T_i and T_j intersect (in at at least one vertex of T). Given a graph G, a set $\mathscr{T}$ of subtrees such that $G(\mathscr{T}) = G$ is termed a *subtree intersection representation* of G. In the rest of this work we refer to the vertices of T as *nodes* to distinguish them from the vertices of G. It is well known that a graph is chordal if and only if it has a subtree intersection representation [4]. Note that the set of trees of the forest T is in one-to-one correspondence with the connected components of $G(\mathscr{T})$.
Minimal representations and maximal cliques: For a node v of T, let $\mathscr{T}_v \subseteq \mathscr{T}$ be the set of subtrees in $\mathscr{T}$ that contain the node v, and let K_v be the set of vertices of G that correspond to the subtrees $\mathscr{T}_v$. It follows from the definitions that K_v is a clique. Moreover, it is known that a chordal graph G has a subtree representation $\mathscr{T}$ in which the nodes of T are in one-to-one correspondence with the maximal cliques of G. Such a representation is termed *minimal* (see also [5]) and the forest T is termed *a clique forest* of G. By definition, $K_u \setminus K_v \neq \emptyset$ and $K_v \setminus K_u \neq \emptyset$ for any two maximal cliques K_u and K_v of a graph G. In particular, this holds whenever G is chordal and uv is an edge of a clique forest T of G.
Let uv be an edge of T where u is a leaf. From the above definitions and facts, it follows that every vertex in $K_u \setminus K_v \neq \emptyset$ is simplicial. We term such a vertex as *leaf-simplicial* vertex of $\mathscr{T}$.

3. The Short Proof

We start with definitions that are needed for our proof.
Given a minimal representation $\mathscr{T}$ of a chordal graph G with T being the union of the subtrees in $\mathscr{T}$ we denote:

- by $d2(\mathscr{T})$ the number of degree-two nodes of T,
- by $L(\mathscr{T})$ the set of leaves of T,
- by $\ell(\mathscr{T}) \stackrel{def}{=} |L(\mathscr{T})|$ the number of leaves of T,
- by $k(\mathscr{T}) \stackrel{def}{=} \max_{u \in L(\mathscr{T})} |K_u|$, the maximum size of a clique of G that corresponds to a leaf of T, and
- by $s(\mathscr{T})$ the number of leaf-simplicial vertices of $\mathscr{T}$.

We associate with every minimal representation $\mathscr{T}$ a quadruple $Q(\mathscr{T}) \stackrel{def}{=} (\ell(\mathscr{T}), -k(\mathscr{T}), -d2(\mathscr{T}), s(\mathscr{T}))$. Denote by $\prec_{LEX}$ the lexicographic order on $\mathbb{Z}^4$ and by $\preceq_{LEX}$ its reflexive closure. We write $\mathscr{T} \prec_{LEX} \mathscr{T}'$ (resp. $\mathscr{T} \preceq_{LEX} \mathscr{T}'$) as a shorthand for $Q(\mathscr{T}) \preceq_{LEX} Q(\mathscr{T}')$ (resp. $Q(\mathscr{T}) \preceq_{LEX} Q(\mathscr{T}')$).

Lemma 3.1. *Let d, ν be two integers. If all the graphs in $\mathscr{M}_{\text{CHORDAL}}(d, \nu)$ are factor-critical then $K_{2\nu+1} \in \mathscr{M}_{\text{CHORDAL}}(d, \nu)$.*

Proof. Among all minimal representations of graphs in $\mathscr{M}_{\text{CHORDAL}}(d, \nu)$ let $\mathscr{T}$ be one such that $Q(\mathscr{T})$ is minimum in $\preceq_{LEX}$. Let $G = G(\mathscr{T})$ and let T be the union of the subtrees in $\mathscr{T}$. By the assumption of the lemma G is factor-critical, thus contains $n = 2\nu + 1$ vertices.
If T consists of one node then G has one maximal clique, i.e., G is a clique and the proof is completed. If T has exactly two nodes, then they are necessarily adjacent, i.e., G consists of two maximal cliques with at least one common vertex. Then this vertex is universal and has degree at most $d-1$. Therefore, $n - 1 < d$, i.e., $n \leq d$. Then, the clique K_n on n vertices is a chordal graph with matching number ν, maximum degree less than d and more edges than G contradicting the assumption that $G \in \mathscr{M}_{\text{CHORDAL}}(d, \nu)$. In the rest of the proof we assume that T has at least three nodes.
We will now present two successive transformations on $\mathscr{T}$ by which we obtain two minimal representations $\mathscr{T}'$ and $\mathscr{T}''$ such that

$$\mathscr{T}'' \preceq_{LEX} \mathscr{T}' \prec_{LEX} \mathscr{T}. \tag{3.1}$$

Denote $G' = G(\mathscr{T}')$, $G'' = G(\mathscr{T}'')$. The transformations will preserve the number of subtrees, thus the number of vertices of the graphs. Therefore, the graphs G' and G'' will be chordal graphs on $n = 2\nu + 1$ vertices. As such, their matching numbers are at most ν.
The transformations ensure that G' is obtained by adding one edge ij to G where j is a simplicial vertex of G, and G'' is obtained from G' by removing one edge ij'. The only vertex whose degree increases after these transformations is j. Since j is simplicial in G it does not have maximum degree. Therefore, $\Delta(G'') \leq \Delta(G) < d$. Clearly, G and G' have the same number of edges. Then $G'' \in \mathscr{M}_{\text{CHORDAL}}(d, \nu)$. Since $\mathscr{T}'' \prec_{LEX} \mathscr{T}$, this is a contradiction to the way $\mathscr{T}$ is chosen.
We now describe the first transformation: Let $u \in L(\mathscr{T})$ be a leaf of T such that $|K_u| = k(\mathscr{T})$ and let v be the unique neighbour of u in T. Let also $\bar{T} = T \setminus \{u, v\}$ be the forest obtained by removing the nodes u and v from T. If K_v contains a simplicial vertex i then it is not of maximum degree. Then adding the edge ij to G will not violate the degree restriction, contradicting the fact that $G \in \mathscr{M}_{\text{CHORDAL}}(d, \nu)$.

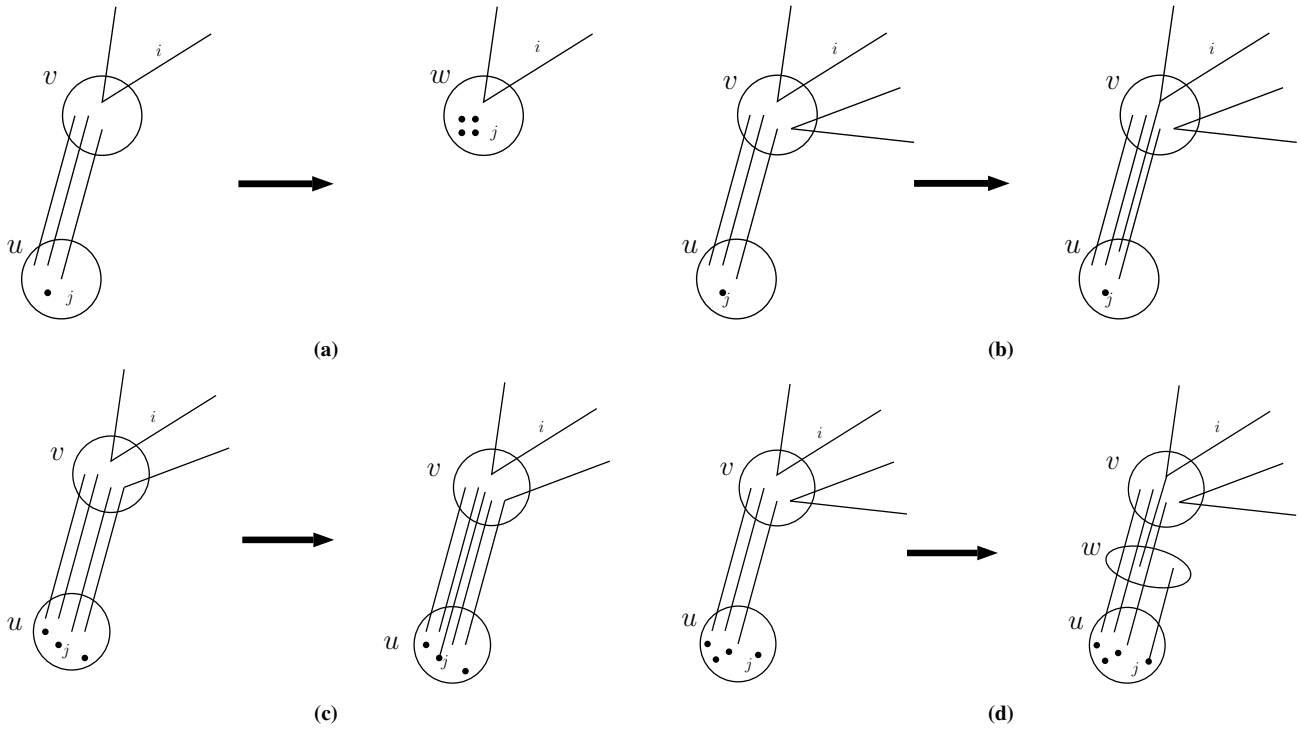

Figure 3.1: The first transformation

Therefore, K_v does not contain simplicial vertices. Consider a vertex $i \in K_v \setminus K_u$. Since i is not simplicial, it has at least one neighbour in $G \setminus K_u \setminus K_v$ In other words, the subtree $T_i \in \mathscr{T}$ that corresponds to vertex i has a non-empty intersection with the forest $\bar{T}$.
We consider four disjoint and complementing cases. Consult Figure 3.1 for illustrations.

(a) $K_u \setminus K_v = \{j\}$ and $K_v \setminus K_u = \{i\}$: In this case we contract the edge uv to obtain a node w and set $K_w = K_u \cup K_v = K_u \cup \{j\}$. If w is not a leaf then $\ell(\mathscr{T})$ decreases. Otherwise, w is a leaf and $|K_w| = |K_v| + 1$, i.e., $\ell(\mathscr{T})$ remains intact and $k(\mathscr{T})$ increases.
(b) $K_u \setminus K_v = \{j\}$ and $K_v \setminus K_u \supsetneq \{i\}$: In this case we add i to K_u, leaving the number of leaves intact and increasing $k(\mathscr{T})$ by one.
(c) $K_u \setminus K_v \supsetneq \{j\}$ and $K_v \setminus K_u = \{i\}$: In this case we add j to K_v decreasing $s(\mathscr{T})$ and leaving the rest of the parameters intact.
(d) $K_u \setminus K_v \supsetneq \{j\}$ and $K_v \setminus K_u \supsetneq \{i\}$: In this case subdivide the edge uv by adding a new node w and set $K_w = (K_u \cap K_v) \cup \{i, j\}$. This does not affect $\ell(\mathscr{T})$ and $k(\mathscr{T})$ and increases $d2(\mathscr{T})$ by one.

In all the above cases we have $\mathscr{T}' \prec_{LEX} \mathscr{T}$ as required.
We now proceed with the second transformation. Let u' be a leaf of $T_i \cap \bar{T}$ that is most distant from v. Let v' be the unique neighbour of u' in $T_i \cap \bar{T}$ (possibly $v' = v$) and let j' be a vertex of $K_{u'} \setminus K_{v'}$. By definition $i \in K_{u'} \cap K_{v'}$. We consider two disjoint and complementing cases. Consult Figure 3.2 for illustrations.

(a) $K_{u'} \setminus K_{v'} = \{j'\}$: In this case we remove i from $K_{u'}$, effectively removing the edge ij' from G'. Note that this transformation does not disconnect G' since we assume that all the graphs in $\mathscr{M}_{\text{CHORDAL}}(d, \nu)$ are factor-critical, thus connected. Therefore, T is not affected by the transformation, leaving $\ell(\mathscr{T})$ and $d2(\mathscr{T}')$ intact. Since i is not simplicial, $s(G)$ is left intact too.
(b) $K_{u'} \setminus K_{v'} \supsetneq \{j'\}$: In this case we subdivide the edge $u'v'$ by adding a new node w' and set $K_{w'} = K_{u'} \setminus \{i\}$. As in the previous case this modification does not disconnect G'. The transformation leaves $\ell(\mathscr{T}')$ intact and increases $d2(\mathscr{T}')$.

Since the transformation does not modify K_u and $|K_u| = k(\mathscr{T}')$ does not decrease. In both of the cases above we have $\mathscr{T}'' \preceq_{LEX} \mathscr{T}'$ as required. □

Observation 3.2. *Let $\mathscr{C}$ be a special hereditary graph class, and d, ν two positive integers, and let G be a graph of $\mathscr{M}_{\mathscr{C}}(d, \nu)$ with maximum number of connected components that are stars and maximum number of connected components subject to this constraint. Let $\nu' > 1$ be the matching number of a connected component G' of G. Then all the graphs in $\mathscr{M}_{\mathscr{C}}(d, \nu')$ are factor-critical.*

Proof. Suppose that $\mathscr{M}_{\mathscr{C}}(d, \nu')$ contains a graph G'' that is not factor-critical. By replacing G' by G'' in G we obtain a graph in $\mathscr{M}_{\mathscr{C}}(d, \nu)$. If G'' contains a connected component that is a star then the resulting graph has one star more than G. If G'' is not connected then the resulting graph has one more connected component than G. If G'' is connected it contradicts Theorem 2.3. □

We are now ready to prove the main result.

Theorem 3.3. *There exists a graph $G \in \mathscr{M}_{\text{CHORDAL}}(d, \nu)$ that is the disjoint union of $(d-1)$-stars and odd cliques.*

Proof. Let G be a graph in $\mathscr{M}_{\text{CHORDAL}}(d, \nu)$ with maximum number of stars and maximum number of connected components subject to this condition. Clearly, every connected component of G that is a star, is a $(d-1)$-star, since otherwise we can add at least one edge to G. Let $G_1, \ldots, G_k$ be the connected components of G that are not stars, and let ν_i be the matching number of G_i for every $i \in [k]$. It is easy to verify that the class of chordal graphs is special hereditary. By Observation 3.2, all the graphs in $\mathscr{M}_{\text{CHORDAL}}(d, \nu_i)$ are factor-critical. By Lemma 3.1, G_i can be replaced by a $K_{2\nu_i+1}$. □

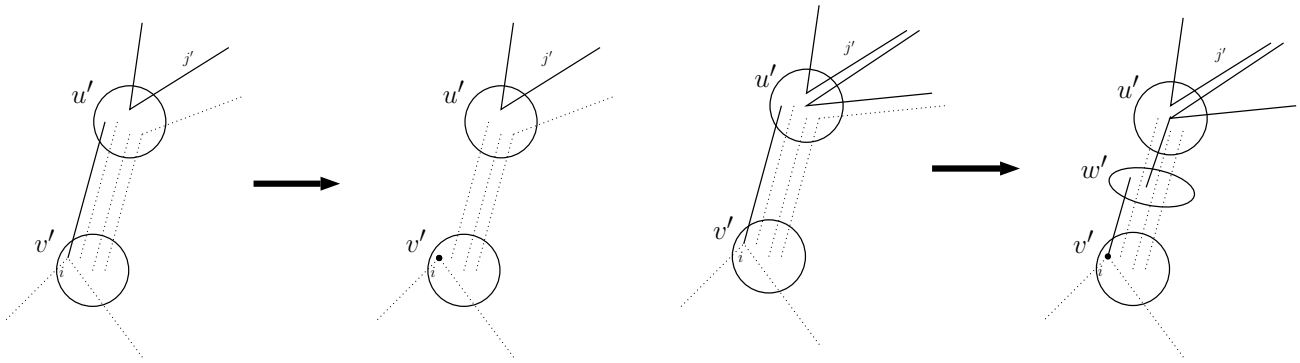

(a) (b)

Figure 3.2: The second transformation

4. Conclusion

We have presented a short proof of the number of edges of an edge-extremal chordal graph. The simplicity of our technique opens room for further improvements. We believe that this proof may be further enhanced to characterize the edge-extremal chordal graphs.

Funding

There is no funding for this work.

Availability of data and materials

Not applicable.

Competing interests

The authors declare that they have no competing interests.

Author's contributions

All authors contributed equally to the writing of this paper. All authors read and approved the final manuscript.

References

[1] V. Chvatal, D. Hanson, *Degrees and matchings*, J. Comb. Theory., Ser. B, **20**(2) (1976), 128–138.
[2] N. Balachandran, N. Khare, *Graphs with restricted valency and matching number*, Discrete Mathematics, **309** (2009), 4176–4180.
[3] J. R. S. Blair, P. Heggernes, P. T. Lima, D. Lokshtanov, On the Maximum Number of Edges in Chordal Graphs of Bounded Degree and Matching Number, Proceeding of the 14th Latin American Symposium on Theoretical Informatics (LATIN 2009), (2020), 600–612.
[4] F. Gavril, *The intersection graphs of subtrees in trees are exactly the chordal graphs*, J. Comb. Theory., **16** (1974), 47–56.
[5] T. Ekim, M. Shalom, O. Şeker, *The complexity of subtree intersection representation of chordal graphs and linear time chordal graph generation*, J. Comb. Optim., **41**(3) (2021), 710–735.

Journal of Mathematical Sciences and Modelling, 5 (2) (2022) 67-79
Review Article

Journal of Mathematical Sciences and Modelling

Journal Homepage: www.dergipark.gov.tr/jmsm
ISSN 2636-8692
DOI: http://dx.doi.org/10.33187/jmsm.1126076

Mathematical Modeling Application in Energy Conversion and Energy Storage

Nagihan Delibaş[1*], Seyyed Reza Hosseini[2] and Aligholi Niaei[1,2]

[1]*Department of Physics, Faculty of Science, University of Sakarya, Sakarya, Turkey*
[2]*Department of Chemical Engineering, University of Tabriz, 5166616471 Tabriz, Iran*
[*]*Corresponding author: caylak@sakarya.edu.tr*

Article Info

Keywords: *Battery, Fuel cell, Mathematical modeling, Simulation, Solar cell, Supercapacitor*
2010 AMS: *97M10, 97M50, 97N60*
Received: *4 June 20222*
Accepted: *10 August 2022*
Available online: *30 August 2022*

Abstract

The use of mathematical modeling to predict and investigate the effect of process variables in the research and engineering field of energy conversion and energy storage has also received special attention from scientists and industrial designers in this field due to their importance in the global economy. This review article investigates the applications of mathematical modeling and simulation in energy conversion and energy storage processes, and finally, with a case study, the application of mathematical modeling in the desired processes to be tested and compared with the reported results in the papers. In the first part, the main emphasis is on energy conversion, especially on the structure of solar cells and fuel cells and mathematical modeling methods, and predicting the effect of operating variables on their performance. The basic principles of modeling solar cells and fuel cells to understand the relationships governing the current, voltage, performance, and power of PV modules are to be discussed. And with a case study, modeling of the process to estimate the performance of PV modules and SOFC in various conditions has been investigated. In the second part, the main focus is on the mathematical modeling of energy storage devices including batteries and supercapacitors. Supercapacitors and batteries are electrochemical energy storage devices that can be charged within a few seconds to a few minutes. This efficient energy storage is based on the electrocatalytic effect of the electrode with a high surface area. The mathematical equations governing the battery and supercapacitor are discussed in the article, and battery and supercapacitor performance are to be simulated as a case study. Due to the Multiphysics nature of energy conversion and storage systems, the simulation is performed in two stages. In the first step, the semiconductor equations are applied and the electrical response of the electrochemical device is modeled. In the second step, if needed, the thermal equations can be entered into the main calculations and the net amount of heat and the temperature profile in the desired device is evaluated. The main goals and ideas of compiling this review article are expressing the importance and role of electrochemical and electrocatalysts in energy production and storage processes and paying attention to the governing mechanism and mathematical equations and highlighting important and common models used in different parts of energy conversion and storage in a coherent article.

1. Introduction

1.1. Why do mathematical modeling?

Mathematical modeling has always been an important activity in all scientific research and development in science and engineering. On another side, the model formulation of qualitative questions and physical phenomena, as mathematical problems was an important motivation

Email addresses and ORCID numbers: caylak@sakarya.edu.tr, 0000-0001-5752-062X (N. Delibaş), sr.hosseini.sr@gmail.com, 0000-0002-0946-7489 (S. R. Hosseini),) aniaei@tabrizu.ac.ir, 0000-0001-5580-4266 (A. Niaei)

for and an integral part of the development of mathematics from the very beginning. In the last decades, the use of mathematics as a very effective tool in problem-solving has gained prominence, mainly due to rapid developments in computing. Computational calculations are particularly important in modeling chemical engineering processes because of the complexity of the physical and chemical laws of these processes. In the chemical processes, heat and mass balances and also momentum balances, are basic mathematical models used in the modeling of chemical reactions engineering. Nevertheless, mathematical equations are the best tools for engineers and scientists to understand important systems and processes. In all engineering contexts, mathematical modeling is a prerequisite such as process control, optimization, mechanistic understanding, design and planning of experiments, simulation instead of costly experiments, feasibility studies, and scale-up of the process.

This article reviews mathematical modeling applications in energy conversion and energy storage. So, it focuses on the energy sector in two sections. In the first section, the major emphasis is on energy conversion, especially on solar cells and fuel cells' structure and methods of modeling and predicting their performances. In the second section, the major emphasis is on energy storage focuses on modeling the structure and performance of batteries and supercapacitors. Supercapacitors and batteries are electrochemical energy storage devices that can be charged in a matter of seconds to minutes. This efficient energy storage is based on an electrolyte's adsorption to a high-surface-area electrode. These marvelous properties led to extensive concerted research into the nature of the storage mechanism, electrode design, and especially new optimized materials. Because of the multi-physics nature of energy conversion and storage systems, the simulation is performed in two steps. In the first step, the semiconductor equations are applied and the electrical response of the electrochemical device is modeled. The second step calculates the thermal equations, while the heat generated in the first step is used as the heat source.

2. Energy Conversion in Solar Cells and Fuel Cells

2.1. Solar Cells

Solar energy is one of the applicable substitutions for non-renewable energy generation sources. Devices that are utilized for solar energy applications are named solar panels which are consisted of solar cells on small scales. These devices are a subset of photovoltaic systems. Their performance is based on two charge carriers named electron with negative charge and hole with positive charge. These opposite charges lead to potential differences through electrodes and accordingly electricity generation. In the practical phase, solar cells are synthesized and deposited in laboratories. Besides, solar panels are fabricated for industrial applications. However, a better understanding of photovoltaic devices' design, simulation, and modeling application are required. It will help researchers to reduce experimental and fabrication errors.

In the case of solar cell simulation, many numerical and modeling software packages were developed. Among them, SCAPS-1D and COMSOL-Multiphysics simulators are common [1, 2]. All of the software packages employ three basic equations including Poisson and electron and hole continuity equations in their software base. In a general perspective, solar cell simulation is performed in three physics containing electrical, optical, and thermal considerations. The base of modeling in the mentioned physics is as below:

2.1.1. Optical section modeling

All of the software packages utilize some basic optical assumptions. Among them, the most popular ones refer to air mass and reflection in the electrodes. Air mass is relevant to the sun's angle with the PV system. In most simulations, the 48° angle or A.M.1.5 is assumed. The other important factor in the optical part refers to the reflection in the front electrode that can be designed in some software packages [3].

2.1.2. Electrical section modeling

In the second physics named electrical part, the Poisson equation (2.1) and the continuity equations for electrons (2.2) and holes (2.3) are solved simultaneously [4, 5]:

Poisson's equation:

$$\nabla.\varepsilon\nabla\phi = -q(p-n+N_D-N_A) \tag{2.1}$$

Electron continuity equation:

$$\frac{\partial n}{\partial t} = \frac{1}{q}\nabla j_n + G_n - U_n \tag{2.2}$$

Hole continuity equation:

$$\frac{\partial p}{\partial t} = \frac{1}{q}\nabla j_p + G_P - U_P \tag{2.3}$$

U_n and U_p are the electron and hole recombination rates, respectively. It should be noted that the recombination factor refers to the dissipation created due to the electron and hole recombination. G_n and $G_p$are the total rate of electron and hole generation, respectively.

One of the parameters required for the calculations of this part is the refractive index and the extinction coefficient related to each layer of the solar cell, which must be considered [6]-[10]:

$$G(y) = \int_{280nm}^{4000nm} -a(\lambda)\,\phi(y,\lambda)\,d\lambda$$

Three types of recombination may occur in solar cells: radiative recombination, SRH (Shockley Reed Hall) recombination, and Auger recombination. Note that the SRH recombination is enabled in the semiconductor module:

$$R_{SRH} = \frac{np - {n_j}^2}{\tau_n \left(n + n_j \exp\left(-\frac{E_T - E_j}{K_B T}\right)\right) + \tau_p \left(p + n_j \exp\left(-\frac{E_T - E_j}{K_B T}\right)\right)}$$

2.1.3. Thermal section modeling

This modeling is set in a few software packages. For instance, the COMSOL software is capable of considering thermal physics in solar cell simulation. The physics of heat transfer in solids for thermal calculations is used. The equation (2.4) governing heat transfer is as follows:

$$-k\nabla^2 T + Q = \rho_p C_p \frac{dT}{dt} \tag{2.4}$$

Where k is the conductive heat transfer coefficient of the material $[W/m.K]$, C_P is the specific heat $[J/(kg.K)]$, ρ is the density $\left[kg/m^3\right]$. Q is the term for heat generation due to various factors. *A* summary of each model was mentioned in the previous sections. They are the basics of the physics of each simulation software.

2.1.4. Case studies

As mentioned above, some of the results of recent studies around the applications of solar cells simulation and modeling tools in some custom solar cells are given.

In 2021, Hosseini et al. [2] studied the effect of different layer properties of a perovskite solar cell such as their thickness and charge carrier density and obtained their optimal parameters using SCAPS-1D software. The optimum cell's final current-voltage curve was represented in Figure 2.1 Another simulation study with the SCAPS-1D tool was performed by Hosseini et al. in 2021 that was based on investigating different configurations of HTL in a custom perovskite solar cell, [11]. They studied three common HTL types, Spiro-OMeTAD, P_3HT, and Cu_2O, and their effects on cell performance in different composite, tandem, and single forms, and their results were compared.

Moreover, other simulation tools were employed by researchers in recent years. For instance, Delibas et al. [1], investigated the effect of using different hole transfer layers, both polymeric and non-polymeric by using COMSOL Multiphysics software. For this purpose, three HTM layers (Spiro-OMETAD, $CuSCN$, P_3HT) have been investigated. The I-V curves of the mentioned structures were collected in Figure 2.1.

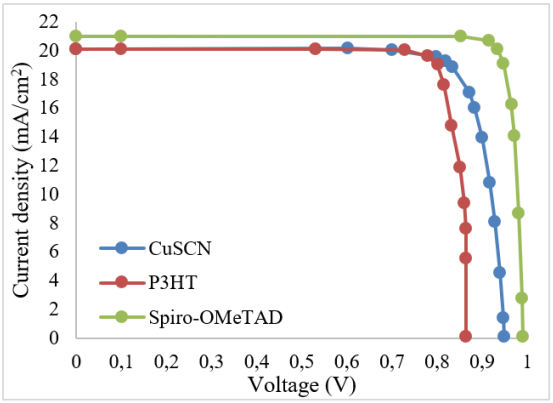

Figure 2.1: Current-Voltage Curve of the Perovskite Solar Cell using different HTMs [1]

A summary of the mentioned studies' performance parameters (electrical-optical physics) was given in Table 2.1.

It should be noted that the parameters mentioned in Table 2.1 including VOC, JSC, FF, and PCE refer to the solar cell's open circuit voltage, short circuit current, Fill Factor, and power conversion efficiency, respectively.

All of the studies mentioned in Table 2.1, were validated with similar experimental data. For instance, according to the data validated for the Au/ Spiro-OMeTAD/ $CH_3NH_3PbI_3$/ TiO_2/ FTO in the mentioned work in the table ([11]), the photovoltaic parameters including V_{OC}, J_{SC}, FF, PCE was $1.08V$, $22.43\ mA/cm^2$, 79.63%, 19.26% for simulation and $0.98V$, $21.20 mA/cm^2$, 77.60%, 18.70% for experimental works, respectively.

In 2021, Bouarissa et al. modeled a CZTS solar cell with the new proposed $ZnO/MoS_2/CZTS$ structure using the SCAPS-1D software package. They performed the optimization of each layer's thickness and obtained a final efficiency of about 23% [12]. In another study, in 2021, Islam et al. studied the numerical modeling of a $CdTe$ solar cell with the WS_2 buffer layer through SCAPS-1D simulation. They obtained an efficiency of 20.55 % [13].

Other simulation tools were employed to perform the numerical modeling of solar cells. In 2021, microcrystalline silicon solar cells were simulated by Plotnikova et al. using TCAD software. In that research, the structures and characteristics of the custom solar cell were

Configuration	Structure	V_{OC} (V)	J_{SC} (mA/cm^2)	FF (%)	PCE (%)	Ref.
simple	Au/ Spiro-OMeTAD/ P_3HT/ $CH_3NH_3PbI_3$/ TiO_2/ FTO with the ultrathin P_3HT polymeric layer	1.18	25.54	88.11	26.52	[2]
simple	Spiro-OMeTAD	1.08	22.43	79.63	19.26	[11]
	P_3HT	0.87	32.09	57.09	15.92	[11]
	Cu_2O	1.08	22.44	81.60	19.77	[11]
composite	$(Spiro\text{-}OMeTAD)_{0.1}(P_3HT)_{0.9}$	1.05	29.59	79.37	24.57	[11]
	$(Spiro\text{-}OMeTAD)0(Cu_2O)1$	1.08	22.44	81.60	19.77	[11]
	$(Cu_2O)_{0.4}(P_3HT)_{0.6}$	1.02	25.00	80.84	20.66	[11]
tandem	$Spiro\text{-}OMeTAD/P_3HT$	1.09	31.47	78.37	26.97	[11]
	$P_3HT/Spiro\text{-}OMeTAD$	1.08	22.43	77.86	18.81	[11]
	$Spiro\text{-}OMeTAD/Cu_2O$	1.08	22.44	81.03	19.63	[11]
simple	Spiro-OMeTAD	21	0.973	82.00	16.80	[1]
	CuSCN	20	0.949	83.00	15.70	[1]
	P_3HT	20	0.720	84.00	12.10	[1]

Table 2.1: The photovoltaic parameters obtained for different perovskite solar cells studies [2].

obtained and the photovoltaic parameters were calculated using the TCAD modeling system [14]. For other modeling tools, a simulation was performed in 2020 by Rasheed et al. using MATLAB software. The simulation was performed around Single-Diode solar cells. In their study, they suggest and analyze two algorithms; a new Inverse Quadratic Interpolation and Illinois for solving the nonlinear equation of a solar cell single diode type with initial value $x0$ and load resistance R varies from 1 to 5 Ω is implemented in MATLAB program. Using five numerical testes examples, the results secured reveal that the suggested algorithm has lesser iterations than the other method (Illinois method), so the accuracy and efficiency of the proposed method are the best [15].

In the case of thermal modeling, in 2019, Saxena et al. [16] presented an extended 3D simulation of heat distribution in perovskite solar cells. They studied the temperature distribution in conventional perovskite solar cells through paired optical-electrical-thermal modules. The wave optical module, the semiconductor module, and the heat transfer in the solid module are coupled in their simulation in the 3-D wizard. The simulation results indicated that the heat generated in the cell is best dissipated from the metallic contact where the $PbI2$ defect forms because of oxidation or decomposition of the perovskite layer at moisture exposure.

In conclusion, it can declaim that simulation can possess many positive effects in understanding the behaviors of solar cells and can help us orientation in solar cell study.

2.2. Fuel cells: Current, temperature, and concentration distribution of a solid oxide fuel cell with COMSOL: 3D modeling

2.2.1. Why is solid oxide fuel cell?

Solid Oxide Fuel Cell (SOFC) is one of the important parts of energy conversion systems. The most significant parts of SOFC are two electrodes and the electrolyte between them. Anode and cathode electrodes should be porous, ion conductor, electron conductor, thermally compatible with electrolytes, and stable in high temperatures. For a good understanding, Figure 2.2 demonstrates the operation of $SOFC$ with H_2 as fuel [17]-[19].

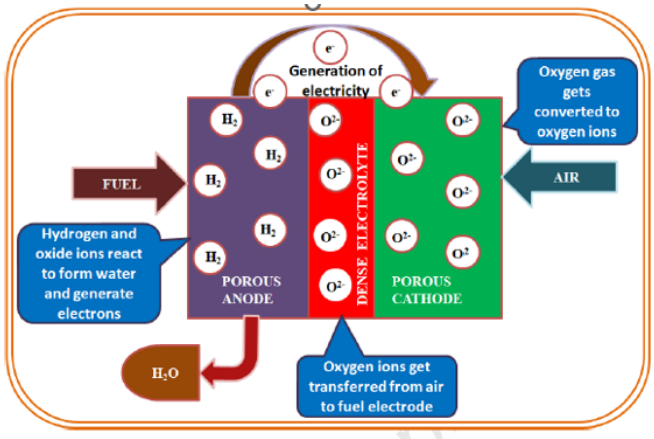

Figure 2.2: The operation of SOFC with H2 as fuel [19].

The main structure of SOFC, which contains the electrolyte has some special properties like being dense, ion conductor, thermally compatible with electrodes, stable in both reduction and oxidation environments, and weak electron conductor or not being an electron conductor at

all. In the cathode, the oxygen reduction reaction (ORR) happens, and then the oxygen transfers to the anode through the electrolyte and anode, where the hydrogen turns to the proton, oxygen ions and protons react and turn to water. Generally, the following mechanisms can be described these phenomena:

$$\frac{1}{2}O_2 + 2e^- \rightarrow O^{2-}$$

$$O^{2-} + H_2 \rightarrow H_2O + 2e^-$$

In this reaction, electrons are released and transferred to the cathode and this way electricity required for transport, or electronic devices can be produced [20]-[23].

2.2.2. Mathematical modeling in SOFC

To simulate SOFC in 3D, to be used the capabilities of COMSOL Multiphysics software to draw models in 2D. At first, a cross-section of the desired SOFC is to be drawn in the work plane, then with the use of Extrude mode, turn the two-dimensional model into a three-dimensional model (Figure 2.3).

In this modeling, the secondary current distribution, gas diffusion in porous media and flow channels, transport of concentrated species, and heat transfer in solids and fluids are considered. The detail of this mentioned section is described in detail below (2.5)-(2.7):

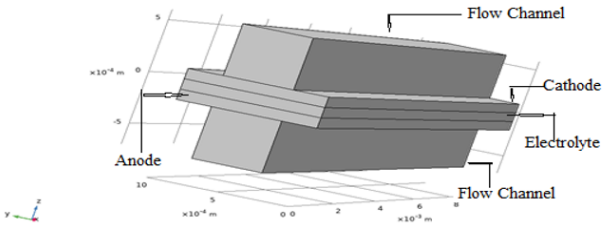

Figure 2.3: Two-dimensional model into a three-dimensional model [18].

Secondary Current Distribution: The relationship between charge transfer and over potential can be described using the Butler-Volmer and Tafel equations as below:

$$i = i_{o.a}\left[\frac{C_{h_2}}{C_{h_{2.ref}}}\exp\left(\frac{0.5F\eta}{RT}\right) - \left(\frac{C_{h_{2o}}}{C_{h_{2.ref}}}\right)\exp\left(\frac{-1.5F\eta}{RT}\right)\right] \tag{2.5}$$

where $i_{o.a}$, F, C_{h2}, C_{h2o} the are the anode exchange current density, the Faraday's constant, molar concentration of H_2 and the molar concentration of H_2O respectively.

The overvoltage is defined by:

$$\eta = \phi_{electronic} - \phi_{ionic} - \Delta\phi_{eq} \tag{2.6}$$

where $\Delta\phi_{eq}$ is the equilibrium potential difference. The cathode charge transfer kinetics is given by:

$$i = i_{0.c}\left[\exp\left(\frac{3.5F\eta}{RT}\right) - x_{o2}\left(\frac{C_t}{C_{o2.ref}}\right)\exp\left(\frac{-0.5F\eta}{RT}\right)\right] \tag{2.7}$$

where $i_{0.c}$ is the cathode exchange current density and $x_{o2}$is the molar fraction of O_2.

Gas diffusion in porous media and flow channel: For gas diffusion in porous electrodes calculation, the Brinkman equation (2.8) is used:

$$\nabla p = -\frac{\mu}{K}v + \mu_e\nabla^2(v) \tag{2.8}$$

where v, μ, and μ_e is the fluid velocity, fluid viscosity, and effective viscosity parameter respectively.

And the weakly compressible Navier-Stokes equation (2.9) is used for modeling gas flows in open channels:

$$\rho\left(\frac{\partial u}{\partial t} + u.\nabla u\right) = -\nabla p + \nabla\left(\mu\left(\nabla u\right) + \left(\nabla u\right)T\right) - \frac{2}{3}\mu\left(\nabla u\right)I) + F \tag{2.9}$$

where u, p, ρ, μ and F are the fluid velocity, fluid pressure, fluid density fluid dynamic viscosity, and external forces respectively [21]-[23].

Transport of concentrated species: The Stefan- Maxwell equation (2.10) is used to modeling of fluid transfer, both bulk transfer and diffusion in porous electrodes (anode and cathode flow channels).

$$\frac{\partial \rho \omega_i}{\partial t} + \nabla.(j_i + \rho \omega_i u) = R_i \tag{2.10}$$

where $\rho\omega_i$, j_i, and R_i denotes the density, the mass fraction molecular mass flux, and reaction rate respectively.

Heat transfer in solids and fluids: The general equation (2.11) of heat transfer intended for the model is given below. In this model, it is used steady state heat transfer and considered the convection heat transfer only for gas channels. In addition, it is ignored radiation heat transfer.

$$\rho.c_p.u.\nabla T = \nabla.(k\nabla T) + Q \tag{2.11}$$

Here Q is the heat generation or consumption, k is the effective thermal conductivity, T is the temperature, and cp is the gas phase-specific heat. The heat generated by electrochemical suction, ohmic polarization, etc. given by (2.12):

$$Q = i.\left(\frac{T.\Delta S_r}{n_e.F} + \eta\right) + \sum \frac{i^2}{\sigma} + \sum \left(r_{ref}.\Delta H_{ref}\right) \tag{2.12}$$

where ΔS_r is the entropy change of the reaction, r_{ref} the reforming reaction rates $\left(in\,mol/m^3 s\right)$, and ΔH_{ref} the enthalpy of the reactions.

The energy equation (2.13) for the anode and cathode channel walls is as follows:

$$n.(-k\nabla T) = h.\left(T_w - T_f\right) \tag{2.13}$$

where T_w is the channel wall temperature and T_f is the fluid temperature and h is the heat transfer coefficient in gas flow channels is calculated by the Nusselt number [24]-[26].

2.2.3. Numerical simulation

Based on the geometry and physics of the problem shown in Figure 2.5, after selecting the appropriate boundary conditions, the fuel cell mesh is adjusted and the model is prepared with mathematical equations that can be solved numerically by the FEM method in COMSOL or any similar software's. It is noteworthy that to increase the accuracy of calculations, the meshing in the electrode and electrolyte sections is finer compared to flow channels.

2.2.4. Case study

To apply the governing mathematical equations in the fuel cell, a sample cell study with certain characteristics has been simulated in the COMSOL environment. In this study, a three-dimensional mathematical model of a SOFC that can show the temperature, concentration, and distribution of current inside the cell and the performance of a solid oxide fuel cell is investigated and analyzed. In addition, the flow pattern parameter and operational variables such as input and output current affect the cell performance. The flow pattern changes from the opposite flow to the simultaneous flow. The results showed that the temperature distribution, flow, and concentration of reactants (O_2 and H_2) are related and wherever the concentration of substances is higher, cell performance and the amount of temperature and flow produced increase. However, solid oxide fuel cell performance is better when the flow pattern is concurrent. The results of the study when the flow pattern was simultaneous, both the cathode and anode currents entered from behind the fuel cell and exited the front of the cell.

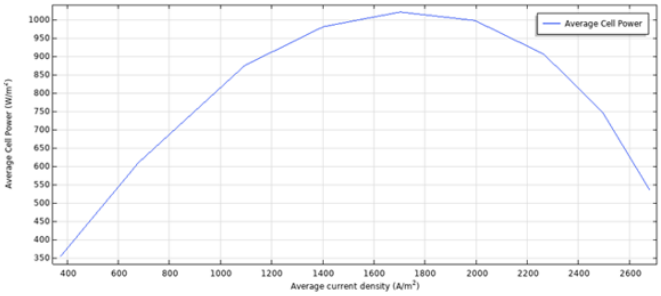

Figure 2.4: Power density- current density plot for counter-current flow pattern [18].

For the reverse flow pattern, the input of the cathode current channel is behind the cell while the input of the anode current channel is in front of the fuel cell. The results of this study in Figures 2.4 and 2.5 show a three-dimensional view of the temperature distribution across the fuel cell [18].

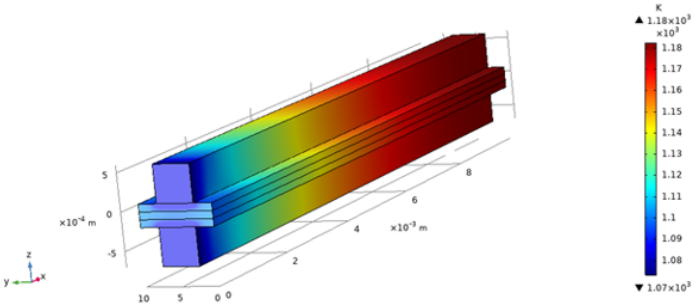

Figure 2.5: Distribution of temperature inside the cell for co-current flow pattern [18].

3. Energy Storage in Batteries and Supercapacitors

3.1. Batteries

The energy stored in the batteries is very important in the energy sector and can be used to power your home and help stabilize the grid. Therefore, batteries are one of the important technology platforms that can be used to improve the state of the world and combat climate change. Electric vehicle battery could be used to help power homes and stabilize the grid. Batteries will increasingly play important role in the future world. different materials in the structure of batteries have different electrochemical properties, and so they produce different results when you put them together in a battery cell. So, in this study, it focused on one of the important batteries with a Lithium-ion structure [27]-[30]. Lithium-ion batteries are an important source of energy storage that attracts scientists and researchers to improve their performance experimentally and computationally. The schematic structure of an electrochemical cell of a lithium-ion (Li-ion) battery is shown in the Figure 3.1. Computational work can help researchers predict and optimize battery performance, saving time and money. The use of mathematical modeling along with powerful simulations such as COMSOL is a great help in designing and creating new ideas in this field. By modeling and simulating different batteries with different geometries and structural materials are designed and their performance is tested in different conditions. High-efficiency batteries are designed by analyzing the results obtained from mathematical modeling and simulation. In this study, the simulation of the discharge mode of the battery connected to the consumer with constant current density is investigated. As a study sample, COMSOL simulation software was performed [31, 32].

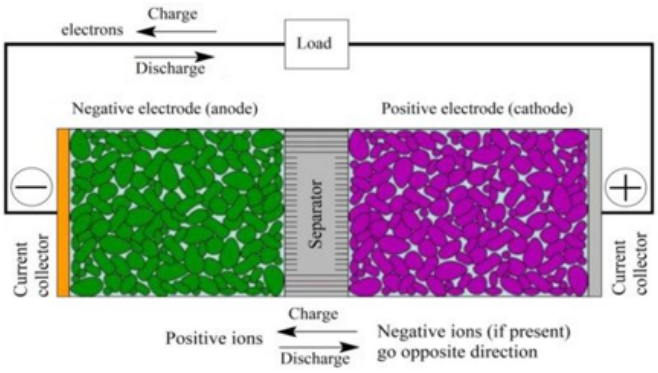

Figure 3.1: The detailed structure of an electrochemical cell of a lithium-ion (Li-ion) battery [28].

3.2. Mathematical models

A simplified structure of a Lithium-ion battery, with the geometry as shown in Figure 3.2 was used and the mathematical model was used based on this two-dimensional structure [33, 34].

The battery in this simulation consists of a negative electrode, an electrolyte, and a positive electrode, in which the negative electrode is applied to the geometry in the form of a surface boundary condition, but the electrolyte and the positive electrode are applied to the geometry of the software. The general module for solving this simulation is a Lithium-ion battery. The main important and relevant equations (3.1)-(3.4) that be used in the COMSOL software are demonstrated below [35]-[37].

$$\frac{\partial c}{\partial t} + \nabla . J_1 = R_1 \tag{3.1}$$

$$\frac{\partial c}{\partial t} + \nabla . J_1 = R_1 \tag{3.2}$$

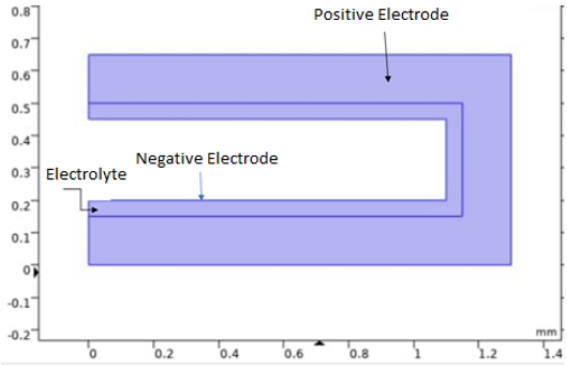

Figure 3.2: Two-dimensional simulation of a Li-ion battery [27].

$$J_1 = -D_1 \nabla c_1 + \frac{i_1 t_+}{F} \tag{3.3}$$

$$i_1 = \sigma_1 \nabla \phi_1 + \frac{2\sigma RT}{F}\left(1 + \frac{\partial \ln f}{\partial \ln c_1}\right)(1 - t_+)\nabla \ln c_1 \tag{3.4}$$

For the electrode and electrolyte, the "Electrode Surface" the suitable boundary condition was used in the COMSOL software. For the electrolyte, $LiPF_6$ has been used, the parameters of which are available in the software database. For the positive electrode, $LiMn_2O_4$ has been used, and the parameters required to simulate this material are also available in the database of COMSOL software. For the Positive electrode, the Porous Electrode boundary condition is added to the volume of the positive electrode in the simulation geometry. As the name implies, in this case, the electrode is considered a porous space and the fine particles penetrate the porous spaces which are considered spherical. The equations (3.5)-(3.12) used in this boundary condition are shown below:

$$\nabla . J_\iota = R_1, R_1 = -\sum_m \frac{v_{Li+,m}\, i_{v,m}}{F} + R_{l,src} \tag{3.5}$$

$$\nabla . i_l = i_{v,total} + Q_l \tag{3.6}$$

$$\nabla . i_s = i_{v,total} + Q_s \tag{3.7}$$

$$J_1 = -D_{l,eff} \nabla c_1 + \frac{i_l t_+}{F} \tag{3.8}$$

$$i_l = -\sigma_{,eff} \nabla \phi_l + \left(\frac{2\sigma_{l,eff} RT}{F}\right)\left(1 + \frac{\partial \ln f}{\partial \ln c_l}\right)(1 - t_+)\nabla \ln c_l \tag{3.9}$$

$$i_s = -\sigma_{s,eff} \nabla \phi_s \tag{3.10}$$

$$D_{l,eff} = {\varepsilon_l}^{1.5} D_l, \sigma_{l,eff} = {\varepsilon_l}^{1.5} \sigma_l, \sigma_{s,eff} = {\varepsilon_{1.5}}^{1.5} \sigma_s \tag{3.11}$$

$$i_{v,total} = \sum_m i_{v,m} + i_{v,dl} \tag{3.12}$$

This boundary condition has two subheadings entitled Particle Intercalation and Porous Electrode Reaction. In the first part, the parameters required for the mass transfer process between the porous spaces of the spherical face electrode are given. It should be noted that Fick's law has been used to establish equations and mass transfer relations. In the Porous Electrode Reaction part, the parameters related to performing the reaction are entered. It should be noted that the kinetic expression of the chemical reaction in this simulation is in the state of Lithium Insertion because this equation requires parameters that are easier to measure, and COMSOL software offers the same state in the default state for lithium-ion batteries.

3.2.1. Case study

In this case study, the discharge time of the battery in two different temperatures in a Lithium-ion battery has been investigated. The battery discharge time is one of the most important parameters in simulating lithium-ion batteries. So, the quantity was examined in the graph of changes in battery potential over time. And in all the simulation processes, battery temperature is considered constant in all stages. In the structure of the battery, the positive electrode is considered to be $LiMn_2O_4$ and $LiPF_6$ is considered the electrolyte, and the negative electrode is considered as the form of a surface boundary condition in the geometry of the battery [27]. The 2D simulated model of a Li-ion battery with COMSOL software was with $50A/m^2$ as discharge current density.

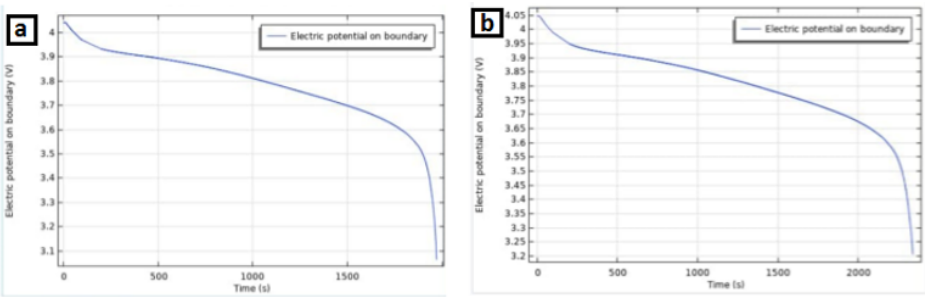

Figure 3.3: Electric potential on boundary versus Time a) at 273°K b) at 350°K [27].

As shown in Figure 3.3 , showing that temperature changes can have a direct effect on battery discharge time, so the higher the temperature, the higher the discharge time. In fact, by increasing the temperature the rate of discharge current enhances, and when the discharge current is considered constant the discharge time increases. The obtained plots demonstrated that the discharge time increases as the battery's temperature enhances. The results are related to the reduction of the resistances inside the battery as the temperature increases which can lead to better performance and higher discharge time of the battery. Also, increasing the temperature improves battery performance. But these batteries are often used in devices such as mobile phones and laptops, so the temperature cannot be considered too high because other components may be damaged. So, there is always an optimal value for the battery temperature depending on its use in devices in which the battery has the maximum efficiency.

3.2.2. Supercapacitor, electrochemical energy storage devices modeling. Temperature, and concentration distribution

3.2.3. Why supercapacitors?

Supercapacitors are electrochemical energy storage devices that can be charged in seconds to minutes and have the distinct advantage of a combination of high output power and high cycle life compared to batteries, as they can be stable for more than $100,000$ cycles. This energy-efficient storage is based on the adsorption of an electrolyte to a high surface electrode. The special properties and superiority of supercapacitors have led to extensive coordinated research on the nature of supercapacitors, storage mechanism, electrode design, and the use of new special and efficient nanomaterials in the construction of supercapacitors. In this regard, mathematical modeling and the use of specialized simulators in this field such as COMSOL and FLUENT are effective and powerful tools in the design, development, and optimization of energy storage devices. And the effect of effective parameters in design and construction, especially the effect of material type on the performance of the supercapacitor, in this modeling and simulation is examined in detail and the performance of the fabricated part can be easily predicted [38, 39].

Certainly, the type of mathematical model used to express the physics of the problem will play a key role in predicting the accuracy of the calculations performed. Farsi and Gobald [40]-[42] investigated the behavior of capacitors consisting of metal oxide nanoparticles using the Lin model et al [43]. In addition, Pech et al. [44] used simulation to investigate the effect of the geometric configuration of tangled surface micro capacitors on their performance. It seems that none of the above models can be used to predict the performance of the new asymmetric capacitor because previous models are designed for capacitors with two identical electrodes. HAO et al. 2016focused on the modeling of the asymmetric supercapacitors that represent the good future of energy storage devices because of their good performance concerning both energy density and power density [45].

They present a mathematical model for the simulation of an asymmetric supercapacitor, that structure consists of a $LiMn_2O_4$ electrode and an activated carbon (AC) electrode. Generally, the dynamic model is used to investigate the effective parameters of supercapacitor structure for the prediction of electrical, and concentration fields and the effect of the thickness of the AC electrode on supercapacitor performance in COMSOL multiphysics. A mathematical model is created to predict the performance of asymmetric capacitors. In this model, the Faraday process and the two-layer process occur at different electrodes. The falls are considered separately with a series of related settings. In the developed dynamic model, both electric field and concentration are included and nonlinear pair equations are solved by the COMSOL Multiphysics technique. Using the model, the effect of the thickness of an AC electrode on the performance of a supercapacitor has been investigated. With this simulation, the production, consumption, and transmission of lithium ions are discussed and energy densities and power densities are calculated [45]. For a proper simulation, it needs to have correct modeling of the system under study and with proper simulation, and can design different supercapacitors with different sizes, geometries, and materials and test their performance in different conditions.

3.2.4. Mathematical models in supercapacitors

For mathematical modeling of supercapacitors, some of the important material balance and electrical balance will be solved simultaneously. In this regard, model equations such as the Continuity equation for material balances of ion transfer, the faradaic process for modeling electric characteristics, the double-layer process, the porosity characteristic of the electrodes, and the ion transport along with the capacitor and inside the particles will be considered. Figure 3.4 presents a sample schematic diagram of an asymmetric supercapacitor in the typical structure that was considered to use in the modeling of a supercapacitor as a case study to be used. Which consists of two different electrodes and a separator and the faradaic redox reaction occurs in the positive electrode during charge/discharge. Mathematical modeling and several simulation methods have been developed to describe and predict the voltammetry of supercapacitor cycles. In this regard, the use of an equivalent resistance-capacitor circuit is one of the most widely used methods for tracking voltammograms, which connects the desired

number of resistors and capacitors in series or parallel. However, resistor-capacitor circuit models with shortcomings such as ion diffusion, non-uniform ion concentration in electrolytes, and electrode morphology are ignored [46].

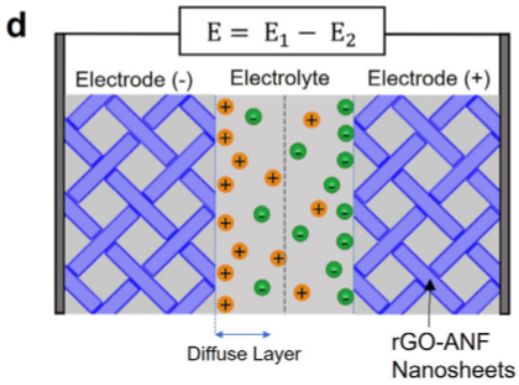

Figure 3.4: Schematic diagram of a typical rGO/ANF nanosheet in a supercapacitor [44].

Generally, the Poisson-Nernst-Planck equation (3.13) is used to calculate the ion transfer across the electrolyte. The local electric potential $E(x,t)$ in the diffuse layer for binary electrolyte solution is determined by the one-dimensional Poisson equation as [43]-[46].

$$\frac{\partial}{\partial x}\left(\in_0 \in_r \frac{\partial E}{\partial x}\right) = -F\sum_{i=1}^{2} z_i c_i \tag{3.13}$$

In this equation, z_i and $c_i(x,t)$ is the charge number of the species $i$and concentration $\left(mol/m^3\right)$, respectively. ε_0 is the vacuum permittivity and ε_r is the relative permittivity of the electrolyte solution. The ion concentration in the electrolyte diffuse layer is calculated by the Nernst-Planck equation (3.14), [46]-[49].

$$\frac{\partial c_i}{\partial t} = \nabla.\left[D_i\left(\nabla C_i + C_i\frac{z_i F}{RT}\nabla E\right)\right] \tag{3.14}$$

where Di is the diffusion coefficient, F is the Faraday's constant, R is the universal gas constant and T/K is the temperature.

On another side, the natural convection in the solution is not considered, since it is assumed that the solution is in a stagnant condition, the diffusion of the electroactive species within the thin layer and near the surface is described by Fick's second law as (3.15), [50]-[52].

$$\frac{\partial C_i}{\partial t} = D_i\frac{\partial C_i}{\partial x} \tag{3.15}$$

At the electrode-electrolyte interface, during cyclic voltammetry measurements, the potential of $E(t)$ is applied linearly with time. Both Faradaic j_F and non-Faradaic (j_c capacitive) processes can take place at an electrode-electrolyte interface. The total current density at the pseudocapacitive electrode-electrolyte interface in equation (3.16) is the sum of j_c and j_F current densities.

$$j_{total} = j_F + j_c \tag{3.16}$$

In above equation (3.16), the capacitive current density j_c is expressed in below equation (3.17) as:

$$j_c = -Cdl\partial E/\partial x, \tag{3.17}$$

The Faradaic current density j_F is expressed by the concentration-dependent Butler-Volmer equation (3.18) as below [50], [53]-[55]

$$j_f = j_0\left\{C_R\,exp\left[\alpha_a\frac{f}{RT}\eta\right] - C_0\exp\left[\alpha_c\frac{F}{RT}\eta\right]\right\} \tag{3.18}$$

Where F, α_a, α_c, j_0 are the Faraday's constant, anodic and cathodic transfer coefficients, and the exchange current density respectively. And the η is calculated by the following equation (3.19).

$$\eta = E - E_{eq} \tag{3.19}$$

The necessary boundary conditions of the model are assumed and established to solve the charge balance and ion transfer balance in the electrode structure. Usually, in using simulation software such as COMSOL it is easy to establish these boundary conditions.

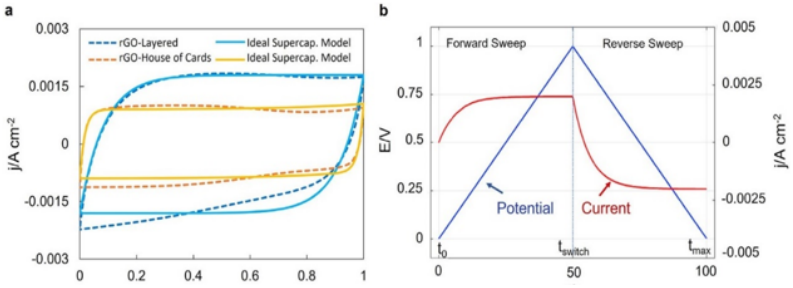

Figure 3.5: The cyclic voltammetry measurements of rGO supercapacitors nanostructures [46].

3.2.5. Case study

To use these mathematical models in supercapacitors as a case study, cyclic voltammetry of a supercapacitor was examined and the results the below [46].
In this case study, the cyclic voltammetry of rGO-ANF (reduced graphene oxide with aramid nanofiber) structural supercapacitors is simulated through COMSOL Multiphysics modeling. The result shows that during cyclic voltammetry, the reaction kinetics can be explained varying by electric potential. The simulation of cyclic voltammetry can be used to determine the more important parameters such as exchange current density, equilibrium potential, and reaction rates by comparing the predicted and measured voltammograms.

4. Conclusion

Considering that the basic principles of both energy conversion and energy storage systems are based on the properties of semiconductors and based on the electrochemical principles of electron transfer, the difference is that in the solar cell system, the principles based on electron-hole transfer and the electrical properties of semiconductors are of interest, and in the case of fuel cells, the principles based on electron-ion transfer and the electrical properties of semiconductors are of interest in these Multiphysics phenomena.

Similarly, it can be stated that the basic principles of both energy storage systems such as batteries and supercapacitors are also based on the electrochemical principles of electron and ion transfer. Therefore, the mathematical equations governing these processes are very similar and often common. Based on this review study, the common mathematical models in electrochemical devices are concluded and described below: Poisson's equation is the common equation between all electrochemical processes. Usually, reaction kinetics related to supercapacitors and fuel cells use the Butler-Volmer equation, which is a common equation in these electrochemical processes.

Also, Ohm's law for electron exchange is common in most electron transfer systems for modeling electron exchange. The relationship between charge transfer and over potential can be described using the Butler-Volmer and Tafel equations. This equation is common for most energy conversion and storage phenomena.

The Stefan- Maxwell and/or Fick's law equations are to be used to modeling of mass transfer, both bulk transfer and diffusion in porous electrodes (anode and cathode flow channels) depending on the structure and type of the energy device. The heat conduction equation is used to model heat transfer phenomena in the energy system with solid/ liquid systems. In general, the heat conduction equation is to be used in the modeling of the temperature profiles of all electrochemical devices such as solar cells, fuel cells, batteries, and supercapacitors.

Acknowledgements

The authors would like to thank the University of Sakarya and the University of Tabriz for their kind contributions.

Funding

There is no funding for this work.

Availability of data and materials

Not applicable.

Competing interests

The authors declare that the current work is derived from the M.Sc. thesis of Seyyed Reza Hosseini, which was Supervised by Prof. Dr. Aligholi Niaei and Advisor Asst. Prof. Dr. Nagihan Delibaş continued, in the Department of Chemical Engineering, University of Tabriz.

Author's contributions

All authors contributed equally to the writing of this paper. All authors read and approved the final manuscript.

References

[1] N. Delibaş, A. Moradi, S. Hosseini, M. Maleki, M. Bahramgour, A. Niaei, *Investigation of the effect of polymeric and non-polymeric materials in the hole transfer layer on the performance of perovskite solar cell*, KSU J. Eng. Sci., **25**(1) (2022), 1–6.

[2] S. Hosseini, M. Bahramgour, N. Delibaş, A. Niaei, *Interface Modification by Using an Ultrathin P3HT Layer in a Custom Perovskite Solar Cell Through SCAPS-1D Simulation,* SAU J. Sci., **25**(5) (2021), 1168–1179.

[3] M. Burgelman, K. Decock, A. Niemegeers, J. Verschraegen, S. Degrave, *SCAPS Manual*, February, 2016.

[4] J. Nelson, *The physics of solar cells,* Imperial College Press, 2003.

[5] A. Hinsch, S. Behrens, M. Berginc, H. Bönnemann, H. Brandt, A. Drewitz, *Material development for dye solar modules: results from an integrated approach,* Prog Photovolt: Res. Appl., **16**(6) (2008), 489–501.

[6] S. Wenger, M. Schmid, G. Rothenberger, A. Gentsch, M. Gratzel, J. O. Schumacher, *Coupled optical and electronic modeling of dye-sensitized solar cells for steady-state parameter extraction*, J. Phys. Chem. C, **115**(20) (2011), 10218-10229.

[7] S. Schöche, N. Hong, M. Khorasaninejad, A. Ambrosio, E. Orabona, P. Maddalena, F. Capasso, *Optical properties of graphene oxide and reduced graphene oxide determined by spectroscopic ellipsometry,* Appl. Surf. Sci., **421**, (2017), 778-782.

[8] J. M. Ball, S. D. Stranks, M. T. Hörantner, S. Hüttner, W. Zhang, E. J. W. Crossland, I. Ramirez, M. Riede, M. B. Johnston, R. H. Friend, H. J. Snaith, *Optical properties and limiting photocurrent of thin-film perovskite solar cells*, Energy Environ. Sci., **8**(2) (2015), 602-609.

[9] P. Pattanasattayavong, G. O. Ndjawa, K. Zhao, K. W. Chou, N. Gross, B. C. Regan, A. Amassian, T. D. Anthopoulos, *Electric field-induced hole transport in copper (I) thiocyanate (CuSCN) thin-films processed from solution at room temperature*, ChemComm, **49**(39), (2013), 4154-4156.

[10] T. H. Anderson, M. Faryad, T. G. Mackay, A. Lakhtakia, R. Singh, *Combined optical–electrical finite-element simulations of thin-film solar cells with homogeneous and nonhomogeneous intrinsic layers*, J. Photonics Energy, **6**(2), (2016), 025502.

[11] S. Hosseini, N. Delibaş, M. Bahramgour, A. T. Mashayekh, A. Niaei, *Performance Comparison of Different Hole Transport Layer Configurations in a Perovskite-based Solar Cell using SCAPS-1D Simulation*, Eur J Sci Technol, (31), (2021), 121–126.

[12] A. Bouarissa, A. Gueddim, N. Bouarissa, H. M. Meherezi, *Modeling of ZnO/MoS2/CZTS photovoltaic solar cell through window, buffer and absorber layers optimization*, Mater. Sci. Eng., B, **263** (2021), 114816.

[13] A. M. Islam, S. Islam, K. Sobayel, E. Emon, F. A. Jhuma, M. Shahiduzzaman, M. J. Rashid, *Performance analysis of tungsten disulfide (WS2) as an alternative buffer layer for CdTe solar cell through numerical modeling,* Opt Mater, **120** (2021), 111296.

[14] E.Y. Plotnikova, A.V. Arsentiev, M. E. Harchenko, *Textured solar cell modeling in TCAD*. In IOP Conf. Series, Mater Sci Eng, **1035**(1), (2021), 012002.

[15] M. Rasheed, M. N. A. Darraji, S. Shihab, A. Rashid, T. Rashid, *The numerical Calculations of Single-Diode Solar Cell Modeling Parameters*, Int J of Phys: Conf. Series **1963**(1) (2021), 012058.

[16] P. Saxena, N. E. Gorji, COMSOL *simulation of heat distribution in perovskite solar cells: coupled optical–electrical–thermal 3-D analysis,* IEEE J Photovoltaics, **9**(6), (2019), 1693-1698.

[17] N. Delibaş, S. Bahrami Gharamaleki, M. Mansouri, A. Niaei, *Reduction of operation temperature in SOFCs utilizing perovskites: Review,* Int. Adv. Res. Eng., **06**(1), (2022), 56-67.

[18] M. Ahangari, *Investigation of Current, Temperature, and Concentration distribution of a Solid Oxide Fuel Cell with Mathematical Modelling Approach*, M.Sc. Thesis, The University of Tabriz, 2021.

[19] S. Hussain, L. Yangping, *Review of solid oxide fuel cell materials: Cathode, anode, and electrolyte*, Energy Transitions, **4**(2) (2020), 113–126.

[20] M.Z. Ahmad, S.H. Ahmad, R.S. Chen, A.F. Ismail, R. Hazan, N. A. Baharuddin, *Review on recent advancement in cathode material for lower and intermediate temperature solid oxide fuel cells application,* Int J Hydrog Energy, **47**(2) (2022), 1103–1120.

[21] T. B. Ferriday, P. H. Middleton, *Alkaline fuel cell technology-A review*, Int. J. Hydrog. Energy, **46**(35) (2021), 18489-18510.

[22] A. M. Abdalla, S. Hossain, A. T. Azad, P. M. I Petra, F. Begum, S. G. Eriksson, A. K. Azad, *Nanomaterials for solid oxide fuel cells: A review,* Renew. Sust. Energ Rev., **82**(1), (2018), 353-368.

[23] N. Kurahashi, K. Murase, M. Santander, *High-Energy Extragalactic Neutrino Astrophysics*, Annu. Rev. Nucl. Part Sci., **72**, 2022.

[24] N. Shaari, S. K. Kamarudin, R. Bahru, S. H. Osman, N. A. Ishak, *Progress and challenges: Review for direct liquid fuel cell*, Int. J. of Energy Research, **45**(5), (2021), 6644-6688.

[25] L. Shu, J. Sunarso, S. S. Hashim, J. Mao, W. Zhou, F. Liang, *Advanced perovskite anodes for solid oxide fuel cells*: A review, Int. J. Hydrog. Energy, **44**(59) (2019), 31275–31304.

[26] M. Singh, D. Zappa, E. Comini, *Solid oxide fuel cell: Decade of progress, future perspectives and challenges*, Int. J. Hydrog. Energy, **46**(54) (2021), 27643-27674.

[27] M. Kooshki, N. Delibaş, S. Bahrami, A. Niaei, *2D Modeling of Lithium-Ion Battery Using COMSOL Multiphysics,* 4th Int. Cong. on Eng Sci Multidiscip Appro, İstanbul, 03-04 Nov. (2022), 603–608.

[28] M. A. Gabalawy, N. S. Hosny, S. A. Hussien, *Lithium-Ion Battery Modeling Including Degradation Based on Single-Particle Approximations,* Batteries **6**(3) (2020), 37.

[29] Z. Feng, W. Peng, Z. Wang, H. Guo, X. Li, G. Yan, J. Wang, *Review of silicon-based alloys for lithium-ion battery anodes*, Int. J. Mineral Metall. Mater., **28**(10) (2021), 1549-1564.

[30] H. Zhang, M. Zhou, C. Lina, B. K. Zhu, *Progress in polymeric separators for lithium ion batteries,* RSC Adv, **5**(109) (2015), 89848–89860.

[31] Y. Miao, P. Hynan, A. Jouanne, A. Yokochi, *Current Li-ion battery technologies in electric vehicles and opportunities for advancements,* Energies, **12**(6) (2019), 1074.

[32] N. Nitta, F. Wu, J. T. Lee, G. Yushin, *Li-ion battery materials: present and future,* Mater Today, **18**(5) (2015) 252–264.

[33] Y. Li, Z. Zhou, W. T. Wu, *Three-dimensional thermal modeling of Li-ion battery cell and 50 V Li-ion battery pack cooled by mini-channel cold plate,* Appl. Therm. Eng., **147** (2019), 829–840.

[34] V. R. Subramanian, V. Boovaragavan, V. D. Diwakar, *Toward real-time simulation of physics based lithium-ion battery models*, Electrochem. Solid-State Lett., **10**(11) (2007), A255.

[35] L. Cai, R. E. White, *Mathematical modeling of a lithium ion battery with thermal effects in COMSOL Inc. Multiphysics (MP) software*, J. Power Sources, **196**(14) (2011), 5985-5989.

[36] D. H. Jeon, S. M. Baek, *Thermal modeling of cylindrical lithium ion battery during discharge cycle,* Energy Convers. Manag. **52**(8-9), (2011), 2973–2981.

[37] A. Lavacchi, U. Bardi, C. Borri, S. Caporali, A. Fossati, I. Perissi, *Cyclic voltammetry simulation at microelectrode arrays with COMSOL Multiphysics*, J. Appl. Electrochem., **39** (2009) 2159–2163.

[38] K. Krois, L. Hüfner, J. Gläsel, B. J. M. Etzold, *Simulative approach for linking electrode and electrolyte properties to supercapacitor performance,* Chemie Ingenieur Technik, **91**(6) (2019), 889–899.

[39] P. Chinnasa, W. Ponhan, W. Choawunklang, *Modeling and simulation of a LaCoO3 Nanofibers/CNT electrode for supercapacitor application,* in J Phys: Conference Series, **1380** (2019), 012101.

[40] H. Farsi, F. Gobal, *Theoretical analysis of the performance of a model supercapacitor consisting of metal oxide nano-particles*, J. Solid State Electrochem., **11**(8) (2007), 1085–1092.

[41] H. Farsi, F. Gobal, *A mathematical model of nanoparticulate mixed oxide pseudocapacitors; part I: model description and particle size effects,* J. Solid State Electrochem., **13**(3) (2009), 433–443.

[42] H. Farsi, F. Gobal, *A mathematical model of nanoparticulate mixed oxide pseudocapacitors; part II: the effects of intrinsic factors,* J. Solid State Electrochem., **15**(1) (2011), 115–123.

[43] C. Lin, J. A. Ritter, B. N. Popov, R. E. White,*A Mathematical Model of an Electrochemical Capacitor with Double Layer and Faradaic Processes*, J. Electrochem. Soc, **146**(9) (1999), 3168.

[44] Pech, D., et al., *Influence of the configuration in planar interdigitated electrochemical micro-capacitors,* J. Power Sources, **230**(2013), 230–235.

[45] D. Pech, M. Brunet, T. M. Dinh, K. Armstrong, J. Gaudet, D. Guay, *Modeling and simulation of a lithium manganese oxide/activated carbon asymmetric supercapacitor,* J. Electron Mater., **45**(1) (2016), 515–526.

[46] S. Aderyani, P. Flouda, S. A. Shah, M. J. Green, J. L. Lutkenhaus, H. Ardebili, *Simulation of cyclic voltammetry in structural supercapacitors with pseudocapacitance behavior,* Electrochim. Acta, **390** (2021), 138822.

[47] C. Lian, D. Jiang, H. Liu, J. Wu, *A generic model for electric double layers in porous electrodes*, J. Phys. Chem. C, **120** (2016), 8704–8710.

[48] M. Kroupa, G. Offer, J. Kosek, *Modeling of supercapacitors: factors influencing performance,* J. Electmchem. Soc, **163**(2016), A2475–A2487.

[49] H. Girard, H. Wang, A. d'Entremont, L. Pilon, *Physical interpretation of cyclic voltammetry for hybrid pseudocapacitors*, J. Phys. Chem. C, **119** (2015), 11349–11361.
[50] H. Wang, L. Pilon, *Accurate simulations of electric double layer capacitance of ultramicroelectrodes,* J. Phys. Chem. C, **115** (2011) 16711–16719.
[51] H. Wang, L. Pilon, *Physical interpretation of cyclic voltammetry for measuring electric double layer capacitances,* Electrochim. Acta, **64** (2012) 130–139.
[52] H. Wang, A. Thiele, L. Pilon, *Simulations of cyclic voltammetry for electric double layers in asymmetric electrolytes: a generalized modified Poisson-Nernst-Planck model,* J. Phys. Chem. C, 117, (2013), 18286–18297. M. Bohner, A. Peterson, (Eds.), Advances in Dynamic Equations on Time Scales, Birkhäuser, Boston, 2003.
[53] A. Bard, L. Faulker, *Electrochemical Methods, Fundamentals and Applications*, Wiley and Sons, New Jersey, (2001), 137–153.
[54] T. Fuller, J. Harb, *Electrochemical Engineering*, Wiley Sons, New Jersey, (2018), 41–87.
[55] J. Newman, K. T. Alyea, *Electrochemical Systems,* Wiley Sons, New Jersey, (2004), 269–315.